A Dinuclear Ru(II) Schiff-Base Complex Catalyzed One-pot Synthesis of Quinolines through Acceptorless Dehydrogenative Coupling of Secondary Alcohols with 2-Nitrobenzyl Alcohol

Gopal Deshmukh, Santosh J. Gharpure, and Ramaswamy Murugavel*

Department of Chemistry, Indian Institute of Technology Bombay, Powai, Mumbai-400076, India;
E-mail: rmv@chem.iitb.ac.in

Abstract: Dinuclear Ru(II) complexes [(*p*-cymene)$_2$(RuCl)$_2$L^1]2X (X = BF_4 (**Ru1**); X = PF_6 (**Ru2**)) and mononuclear [(*p*-cymene)(RuCl)L^2]BF_4 (**Ru3**) (where L^1 = N,N'-(3,3',5,5'-tetraisopropyl-[1,1'-biphenyl]-4,4'-diyl)bis(1-(pyridin-2-yl)methanimine); L^2 = N-(2,6-diisopropyl-phenyl)-1-(pyridin-2-yl)-methanimine) have been synthesized and characterized by spectroscopic and analytical techniques. Dinuclear **Ru1** and **Ru2** orchestrate direct transformation 2-nitrobenzyl alcohols to quinolines under mild conditions with significant efficiency even when employed at a minimal catalyst loading of 0.1 mol%. Proportional experiments carried out with the corresponding mononuclear complex **Ru3** by keeping the Ru content same (0.2 mol% of **Ru3**) reveal superior activity by the bimetallic system **Ru1** for the one-pot quinoline synthesis. Late-stage functionalization of bioactive steroids and scale-up synthesis, demonstrate the practical applicability of the present catalyst system. A probable mechanism of this conversion is proposed based on trapping of many of the intermediates by ESI-mass spectroscopy. These mechanistic studies have further been substantiated by React-IR studies by monitoring the progress of the reaction in real-time.

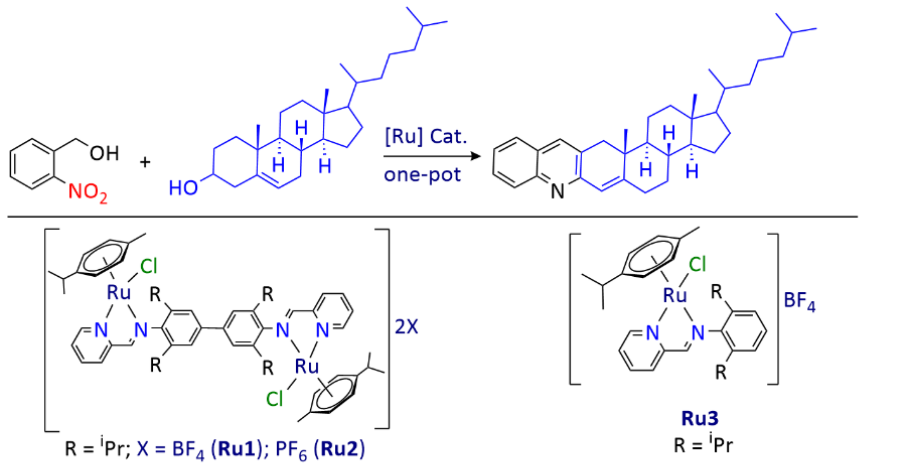

Introduction

Development of simple and efficient synthetic protocols for N-heterocyclic compounds has remained a priority in synthetic organic chemistry due to their prevalence in biologically essential molecules. Among these, quinoline derivatives have gained notable significance in particular and been utilized as a part of various biologically active molecules.[1,2] The historical importance of quinolines stems from their demonstrated antimalarial activity, which can be traced back to the isolation of quinine from the alkaloid mixture found in the bark of the Cinchona tree (Figure 1).[3,4] This significant episode triggered synthesis of a multitude of artificial quinoline derivatives, each of which with unique molecular and pharmacological properties. These derivatives continue to find pertinence across pharmaceutical products, flavoring agents, agrochemicals, dyes, etc. and hence hold a prominent position within synthetic chemistry.[4–9]

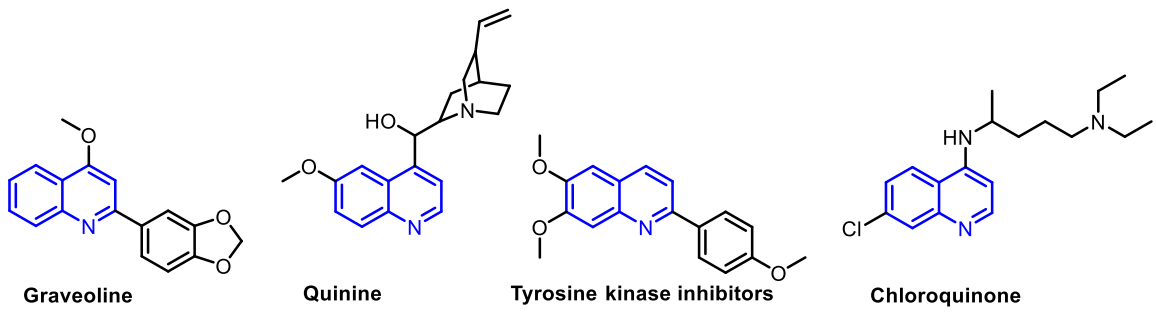

Figure 1. Examples of biologically important quinoline derivatives.

Methodologies which have been already established for quinoline synthesis are summarized in Scheme 1. For example, the Friedlander reaction is the conventional method that is commonly employed to synthesize quinoline derivatives.[10,11] This process relies on thermal condensation of 2-aminobenzaldehydes or 2-aminophenyl ketones with another carbonyl compound that contains acidic α-methylene protons. The reaction can be conducted under either acidic or basic conditions.[12–15] However, a notable challenge arises from the instability of the precursor 2-aminobenzaldehydes and related compounds, which are prone to undergo polymerization through self-condensation reactions at room temperature, necessitating their storage and handling at low temperatures. Moreover, the Friedlander reaction suffers from limited selectivity and atom utilization efficiency.[11] As a result, the pursuit for methods that are both atom-efficient and environmentally sustainable for synthesizing quinoline derivatives has become highly desirable.[16]

During the past few years, the metal-catalyzed acceptorless dehydrogenative coupling (ADC) methodology has become an attractive alternative method.[16–18] This approach has gained enough traction due to its utilization of easily accessible and manageable alcohols as alternative substrates, thus rendering reactions environmentally friendlier and sustainable. Additionally, this strategy also reduces potential side reactions and improves selectivity. Recent studies have explored dehydrogenative strategies involving the reaction of 2-aminobenzyl alcohols with ketones or alcohols, employing various monometallic complexes built from elements such as Ni, Mn, Co, Ru, Rh, Ir, and Pd.[19–29] However, it is worth highlighting that there has been a relative lack of exploration into the synthesis of C-2-substituted quinolines starting directly from 2-nitrobenzyl alcohol using secondary alcohols.[16,30]

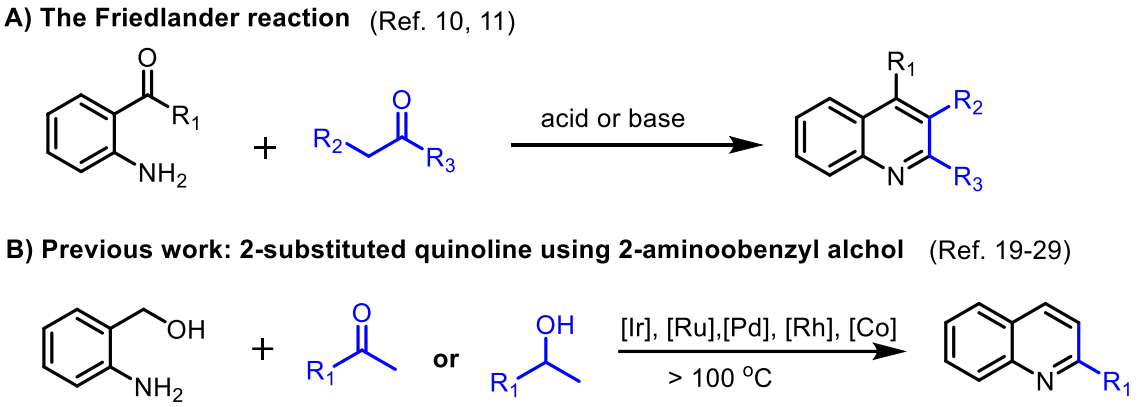

Scheme 1. Representation of previous metal-catalyzed methodologies for quinoline synthesis

Direct synthesis of quinolines from 2-nitrobenzyl alcohol and secondary alcohols is currently limited to only four reports (Scheme 2).[31] While one of these systems reported by Maji et al., employs an expensive iridium cyclopentadienyl complex,[31] the other three reports deal with iron-based catalytic systems. For example, Xie *et al*. showcased quinoline synthesis from 2-nitroaryl alcohol by employing $Ru_3(CO)_{12}$ with expensive 1,1′-bis(diphenyl phosphino)ferrocene (dppf) in the presence of potassium tert-butoxide as the catalytic system.[32] Wang *et al.* developed an iron-catalyzed (dppf) condensation approach for quinolines from 2-nitrobenzyl alcohol in the presence of diisopropylethylamine (DIPEA).[33] More recently, Chun *et al.* have shown that a cyclopentadienone iron complex can be employed for the synthesis of quinolines and quinolones through transfer hydrogenative condensation of ortho-nitrobenzyl alcohols in the presence of trimethylamine oxide (TMAO).[34] It is important to emphasize that

these methodologies, though effective, require harsh reaction conditions such as high temperature (120-160 ^{o}C), longer reaction times (18-48 h), and large catalyst loading (1.5-5 mol%), resulting in moderate yields of quinolines. Besides, the need for extra additives limits the substrate scope while the use of air and moisture sensitive toxic phosphine ligands remains a challenge for further developments in this field (Table S1). One way to tackle such a complex combination of challenges would be to design catalytic systems that can operate under mild conditions with a low catalyst load and still exhibit high selectivity for the one pot production of quinolines from 2-nitrobenzyl alcohol or 2-aminobenzyl alcohol.

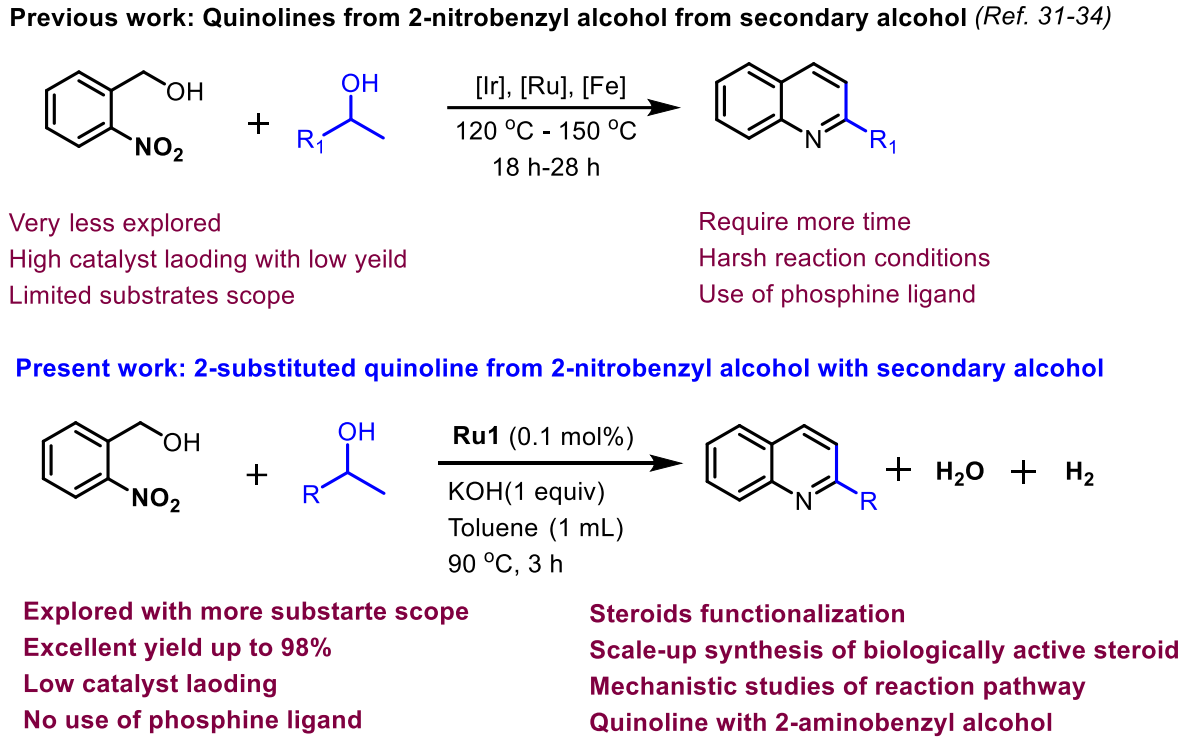

Scheme 2. Representation of previous and present work for synthesis of quinolines from 2-nitrobenzyl alcohol.

Besides, bimetallic catalysts can enhance the rate and selectivity of the catalyzed reaction to a significant level compared to their mononuclear counterparts.[35–37] Improved efficiency of a bimetallic catalyst compared to its monometallic analog is often ascribed to cooperative interactions between the metal centers apart from any additional electronic communication through the bridging organic ligands. Thus, several examples of bimetallic catalysts have been reported for various organic transformations such as hydroformylation,[38] hydroelementation of alkynes,[39] disproportionation of formic acid to methanol,[40] hydroamination,[41] propargylic reduction and substitution reactions.[42,43] For example, Yu and

co-workers have shown that bimetallic ruthenium pincer complexes are more active than a monometallic complex for transfer hydrogenation of ketones.[44–46] Ni-bimetallic complex of Uyeda and co-workers outperforms its mononuclear analog for the hydrosilylation.[47] Similarly, Pernik and co-workers have demonstrated that a bimetallic rhodium complex is more active than a monometallic catalyst for hydrosilylation.[37] Pratihar and co-workers have demonstrated that the cooperativity of a bimetallic Co-Mn catalyst is responsible for its increased catalytic activity in β-alkylation reactions.[48]

Although bimetallic catalysts have exhibited remarkable performance for various organic transformations, one-pot synthesis of quinolines either from 2-nitrobenzyl alcohol or 2-aminobenzyl alcohol has never been investigated by employing a bimetallic catalyst to evaluate any improved catalytic efficiency. The present work reports for the first time the use of bimetallic ruthenium complexes (**Ru1** and **Ru2**) for one-pot synthesis of quinolines using ADC strategy from 2-nitrobenzyl alcohol (or 2-aminobenzyl alcohol) under mild conditions, apart from providing meaningful comparisons with the catalytic performance of its mononuclear counterpart (**Ru3**). The same catalytic approach was also employed for late-stage functionalization of biologically active steroid derivatives to highlight its practical applications. To delve into plausible mechanism, we have conducted investigations through controlled experiments and in spectroscopic analysis.

Results and Discussion

Synthesis and Spectral Characterization

Condensation of either 2,2',6,6'-tetraisopropylbenzidine[49] or commercially available diisopropylaniline with pyridine-2-carboxyldehyde produces ligands N,N'-(3,3',5,5'-tetraisopropyl-[1,1'-biphenyl]-4,4'-diyl)bis(1-(pyridin-2-yl) methanimine) ($\mathbf{L^1}$) and N-(2,6-diisopropylphenyl)-1-(pyridin-2-yl)methanimine ($\mathbf{L^2}$), respectively.[49,50] By combining these ligands with a ruthenium p-cymene precursor complex, new catalytic systems have been prepared in good yields by adopting synthetic protocols used earlier for other ruthenium Schiff base complexes.[51–54] In a typical synthesis, $[Ru(p\text{-cymene})(\mu\text{-Cl})Cl]_2$ reacts with $\mathbf{L^1}$ in the presence of sodium tetrafluoroborate or ammonium hexafluorophosphate in ethanol at room temperature to produce **Ru1** or **Ru2** (Scheme 2). Similarly, the use of $\mathbf{L^2}$ produces **Ru3**. Crude products precipitate out as dark red, yellow, and red solids respectively. The new complexes

were recrystallized from ethanol:acetone (4:1 v/v) mixture and further characterized by spectroscopic and analytical techniques.

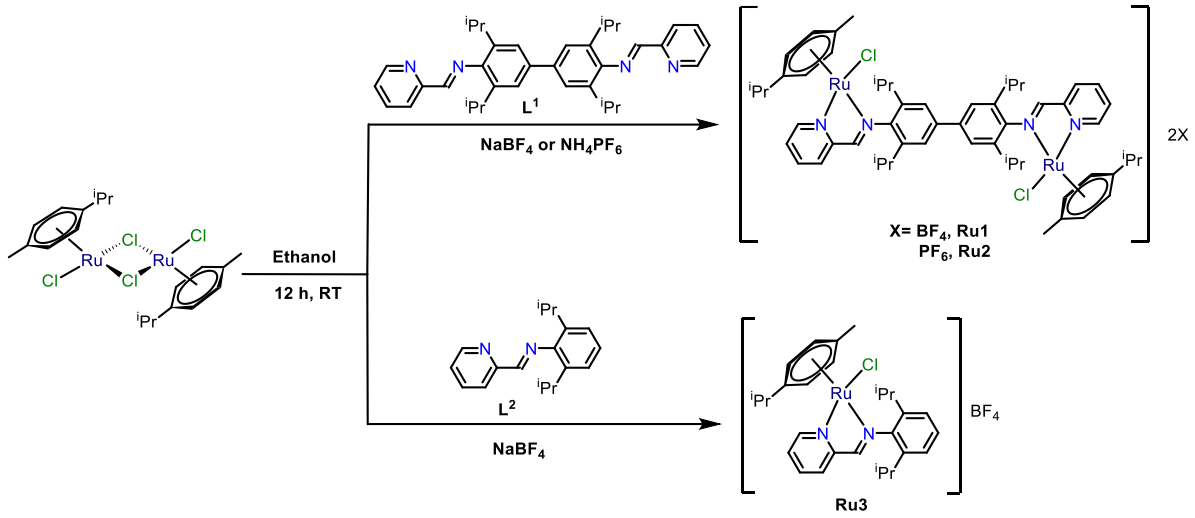

Scheme 2. Synthesis of complexes **Ru1**, **Ru2,** and **Ru3**.

FT-IR spectra revealed significant peaks at 1630 cm^{-1} for **Ru1**, 1632 cm^{-1} for **Ru2**, and 1636 cm^{-1} for **Ru3**, serving as a clear indicator for the presence of Ru-N=C- linkage. These peaks displayed a discernible shift compared to bands observed for the C=N linkages in the ligands (Figure S1). This shift effectively supported the formation of the metal ligand (Ru-N-) bond, highlighting the transfer of electron density from Ru(II) to the Schiff base ligand. ESI-MS spectroscopy confirms the formation of the desired products in each case through the presence of corresponding intense molecular ion peaks at *m/z* 1159.31 for **Ru1** (Figure S2), at *m/z* 1217.25 for **Ru2** (Figure S5) and at *m/z* 537.16 for **Ru3** (Figure S10) in their spectrum, with the expected isotope pattern. Both ^{1}H and ^{13}C NMR spectroscopic studies further confirm the spectral purity of these compounds. For example, in the ^{1}H NMR spectrum of all the three complexes exhibit five doublets for the methyl protons of the isopropyl groups in the range δ1.04-1.59 ppm, providing evidence for the non-equivalence of the isopropyl groups on the rigid complex framework. Correspondingly, two septets are observed in the range δ 3.89-2.55 ppm, distinctly attributing to the isopropyl groups of *p*-cymene and benzidine moiety. Four doublets in the region δ 6.10–5.32 ppm (upfield shift from free cymene confirms Ru-cymene bond formation) represent phenyl protons of the *p*-cymene ring (Figure S3, S6 and S9). ^{13}C NMR spectral (Figure S4, S7 and S10) and the remaining ^{1}H NMR spectral signals are in consistent with the desired product.

The UV-visible spectra of **Ru1**, **Ru2** and **Ru3** were recorded in the range 200-800 nm in dichloromethane at room temperature to understand the electronic structure and the coordination mode of the metal center. The spectra exhibit two distinct absorption maxima, one in the range 250-280 nm and the other in the range 320-350 nm (Figure 2). These bands were assigned to the intra-ligand transition originating from $\pi \rightarrow \pi^*$ and $n \rightarrow \pi^*$ transitions of the ligands. In the cases of **Ru1** and **Ru2**, a single absorption broad band around 380 nm was associated with $d\pi \rightarrow \pi^*$ charge transfer transition and was attributed to a metal-to-ligand charge transfer (MLCT) charge transfer transition (Figure 2).[54,55]

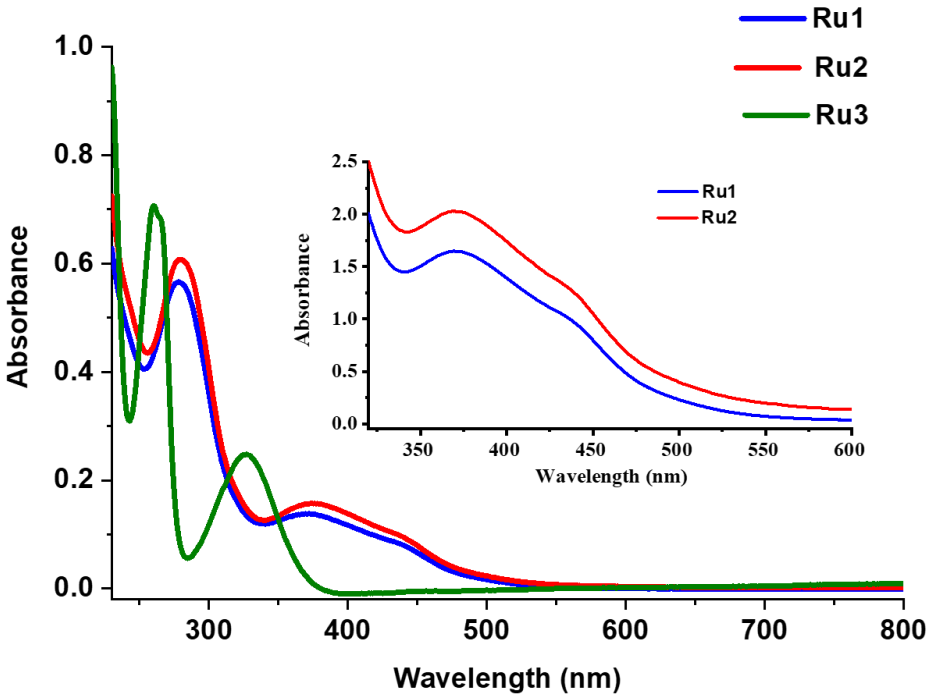

Figure 2. UV–vis spectra of the complex **Ru1**, **Ru2,** and **Ru3** in dichloromethane. **Ru1** [λ_{max} (nm), $\varepsilon(\times 10^4\ M^{-1}\ cm^{-1})$ $(4.1\times 10^{-3}$ M); 277 (13.7), 373 (3.3), 436 (1.6)], **Ru2** [λ_{max} (nm), $\varepsilon(\times 10^5\ M^{-1}\ cm^{-1})$ $(1.3\times 10^{-2}$ M); 278 (4.1), 375 (1.0), 441 (0.6)], **Ru3** [λ_{max} (nm), $\varepsilon(\times 10^5\ M^{-1}\ cm^{-1})$ $(0.99\times 10^{-3}$ M); 259 (7.1), 326 (0.3)].

Molecular structure of Ru1 and Ru3

Single crystals of **Ru1** and **Ru3** complexes suitable for X-ray diffraction analysis were grown by recrystallization of crude product from ethanol:acetone mixture (3:2) under ambient conditions by slow evaporation of the solvent. In both the complexes, the Ru centers adopt pseudo-tetrahedral geometry (piano stool type). The structures of the cationic part of both the complexes along with selected bond lengths and angles are shown in Figure 3 and Figure 4. These metal ions are chelated by pyridyl imine (NN chelate) and are additionally coordinated a chloride ligand and *p*-cymene moiety which is bound in the η^6 fashion. The bond Ru-N, Ru-Cl and Ru-

C(centroid) distances observed for both the complexes are comparable to those reported in the literature (Table S2 and Table S3).[52] The Ru(1) to Ru(2) end-to-end length in **Ru1** complex is 12.772 Å. The presence of ^{i}Pr and *p*-cymene groups induces to non-planarity in the complex due to their steric bulk. Additionally, the two phenyl rings within the **Ru1** deviate from coplanarity, exhibiting torsional angle (twist angle) of 36.23 (5)^{o} between C(24)-C(19)-C(10)-C(11). This non-coplanar arrangement enhances the overall non-planar nature of the **Ru1** complex, rendering it pseudo-C_2-symmetric (Figure 3).

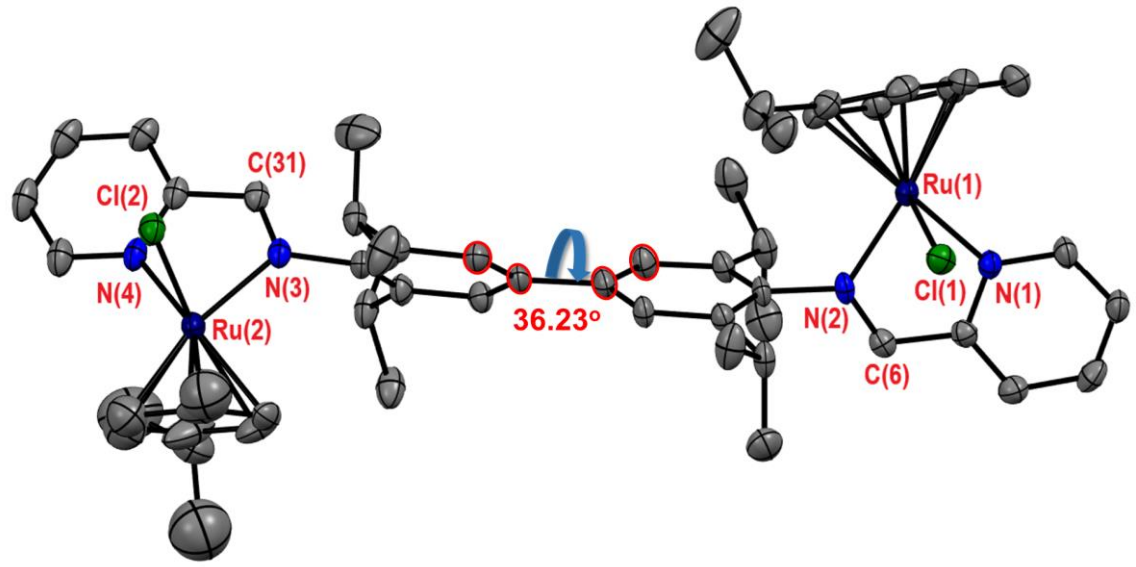

Figure 3. Molecular crystal structure of **Ru1** with 50% probability thermal ellipsoid. Anions, solvent molecules and hydrogen atoms are omitted for clarity. Selected bond lengths (Å) and bond angles (°) for **Ru1**: Ru(1)-Cl(1); 2.397(1), Ru(1)-N(1); 2.103(4), Ru(1)-N(2); 2.112(4), Ru(2)-Cl(2); 2.092(4), Ru(2)-N(4); 2.099(4), Ru(2)-N(3); 2.092(4), N(2)-C(6); 1.288(6), N(3)-C(31); 1.292(7) Å, N(1)-Ru(1)-Cl(1); 81.7(1), N(1)-Ru(1)-N(2); 75.99(1), N(2)-Ru(1)-Cl(1); 89.5(1), N(3)-Ru(2)-Cl(2); 77.1(1), N(4)-Ru(2)-Cl(2); 89.8(1) °.Centroid of *p*-cymene to Ru distance for Ru(1) 1.694(5) Å and Ru(2) 1.698(5) Å in **Ru1** complex. For additional bond lengths and angles, see Table S2.

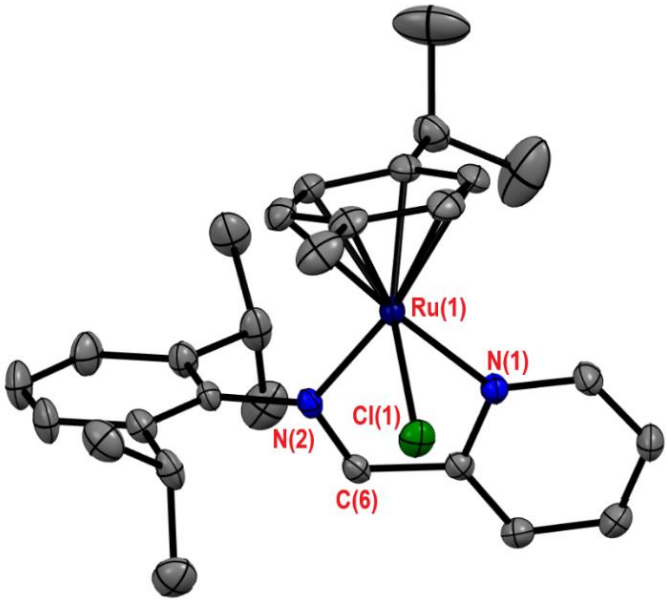

Figure 4. Molecular crystal structure of **Ru3** with 50% probability thermal ellipsoid. Anions, solvent molecules and hydrogen atoms are omitted for clarity. Selected bond lengths (Å) and bond angles (°) for **Ru3:** Ru(1)-Cl(1); 2.3972(8), Ru(1)-N(2); 2.099(2), Ru(1)-N(1); 2.090(1), N(2)-N(2); 1.285(3) Å, N(2)-Ru(1)-Cl(1); 87.88(5), N(1)-Ru(1)-N(2); 77.06(7), N(1)-Ru(1)-Cl(1); 79.60(6)°. Centroid of *p*-cymene to Ru distance for Ru(1) in **Ru3** is 1.693(4) Å. For additional bond lengths and angles, see Table S3.

Optimization of catalytic conditions for coupling of 2-nitrobenzyl alcohol with secondary alcohols

To explore the catalytic activity of bimetallic Ru(II) complexes, first the reaction conditions were optimized using **Ru1** complex. Various reaction parameters were assessed for the model reaction of 1-phenylethanol (**1a**) with 2-nitrobenzyl alcohol (**2a**). The reaction was conducted in a round bottom flask in open-air atmosphere. No special arrangement for removing H_2 from the resulting reaction mixture was needed for this reaction to proceed. Initially, the reaction was conducted by employing **Ru1** of 1 mol% at 90 °C with KOH (1 equiv.) as a base in water, and the expected product 2-phenylquinoline (**3a**) was formed in 61% yield. The use of solvents such as methanol, dioxane, THF, and acetonitrile further lowering the yield of **3a** (Table 1, entries 1-6). However, when the reaction was carried out in toluene using 0.1 mol% of **Ru1** produced **3a** in 93% yield which makes it an ideal choice of solvent. Further, model reactions in isopropanol using **Ru1** catalyst loading of 1 mol% offered a mixture of 2-methylquinoline and 2-phenylquinoline (**3a**) in 41% and 43%, respectively (due to the side reaction with acetone which was formed in-situ from isopropanol). An investigation into the effect of the base (required to carry out alcohol deprotonation) with **Ru1** loading of 1

mol% showed that KOH (93%) is superior when compared to ^{t}BuOK (79%), NaOH (51%), K_2CO_3 (29%), and Cs_2CO_3 (23%) (Table 1, entry 7-10). The reaction failed to proceed in the absence of a base, highlighting the necessity of a base for the reaction. After optimizing the base and solvent, a model reaction was performed at 110 °C for 3 hours using 0.1 mol% of **Ru1** in toluene along with KOH, yielding **3a** in 94%. Lowering the catalyst loading from 0.1 mol% to 0.01 or 0.001 mol% reduces the selectivity for the desired product **3a** formation (Table 1, entries 17 and 18). No significant change in yield was noticed upon lowering the reaction temperature up to 90 °C, however further lowering resulted in decreased yield of **3a**. Reactions carried out either in the absence of catalyst **2a** or KOH did not produce any products (Table 1, entries 19 and 20). Based on the above experimental results, KOH as a base in toluene with 0.1 mol% of **Ru1** for 3 hours at 90 °C was chosen as the optimum reaction condition (Table 1, entry 13).

Optimal conditions were further used to screen the most effective catalyst among complexes **Ru1, Ru2, Ru3,** and [Ru(*p*-cymene)(μ-Cl)Cl]$_2$ (Figure 5). The model reaction with bimetallic **Ru1** and **Ru2** with 0.1 mol%, afforded **3a** in 91% and 93% yield respectively. Whereas loading 0.2 mol% of monometallic **Ru3** as the catalyst yields 39% of **3a** (Table 2). Additionally, the reaction did not proceed in the presence of [Ru(*p*-cymene)(μ-Cl)Cl]$_2$. Conclusively, bimetallic complexes **Ru1** and **Ru2** outperform monometallic **Ru3** in terms of catalytic activity, which can be attributed to the cooperative effect of the bimetallic complex.

Table 1. Optimization of reaction conditions with **Ru1** for coupling of 2-nitrobenzyl alcohol with 1-phenylethanol. Reaction conditions: 2-nitrobenzyl alcohol (1 mmol), 1-phenyl ethanol (2 mmol), solvent (1 mL), base (1 equivalent).

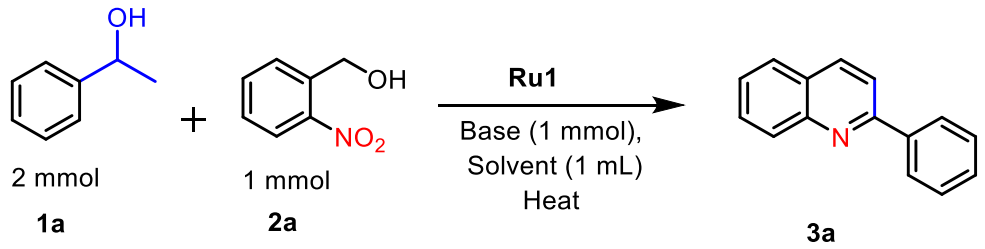

Sr. no	Catalyst (mol%)	Temp (^{o}C)	Solvent (1 mL)	Base	Time (h)	Conversion (%)	Yield (%)	TON	TOF (h^{-1})
1	1	90	H_2O	KOH	12	69	61	62	-
2	1	60	MeOH	KOH	12	trace	trace	trace	-
3	1	100	THF	KOH	12	73	51	51	-
4	1	100	Dioxane	KOH	12	75	42	42	-
5	1	100	Acetonitrile	KOH	12	29	19	19	-
6	1	90	^{i}PrOH	KOH	12	89	43	43	-
7	1	110	Toluene	^{t}BuOK	12	91	79	79	-
8	1	110	Toluene	NaOH	12	67	51	51	-
9	1	110	Toluene	K_2CO_3	12	31	23	23	-
10	1	110	Toluene	Cs_2CO_3	12	37	29	29	-
11	0.1	110	Toluene	KOH	3	100	94	940	313
12	0.1	100	Toluene	KOH	3	100	93	930	310
13	**0.1**	**90**	**Toluene**	**KOH**	**3**	**100**	**93**	**930**	**310**
14	0.1	90	Toluene	KOH	2	96	84	840	420
15	0.1	90	Toluene	KOH	1	88	70	700	700
16	0.1	80	Toluene	KOH	3	92	89	890	290
17	0.01	90	Toluene	KOH	3	98	82	8200	2733
18	0.001	90	Toluene	KOH	3	84	67	67000	22333
19	0.0	90	Toluene	KOH	3	NR	NR	-	-
20	0.1	90	Toluene	-	3	NR	NR	-	-

Inspired by the optimization results, we have focused on the synthesis of various quinoline derivatives using **Ru1** as a catalyst, with a specific emphasis on how different substrates impact the outcomes of the reactions (Scheme 3). The investigation was primarily aimed at probing the effect of electron-withdrawing and electron-donating groups on the aromatic ring of the substrate 1-phenylethanol. Electron-donating substituents, such as methyl and methoxy led to the formation of desired quinoline products **3b** and **3c** in 90 and 92%, respectively. On the other hand, electron-withdrawing substituents such as -F, -Cl, -Br, and -I on the *para*-position of the aromatic ring yielded **3d**, **3e**, **3f**, and **3g** in 73, 80, 84, and 87% quinolines, respectively. The yield of **3d** and **3e** is comparatively lower and it is attributed to the electronic effects that influence the reactivity.

Table 2. Screening of catalyst

Sr. no	Catalyst	mol %	Conversion (%)	Yield (%)
1	Ru1	0.1	100	93
2	Ru2	0.1	100	91
3	Ru3	0.2	46	39
4	[Ru(*p*-cymene)(μ-Cl)Cl]$_2$	0.1	NR	NR

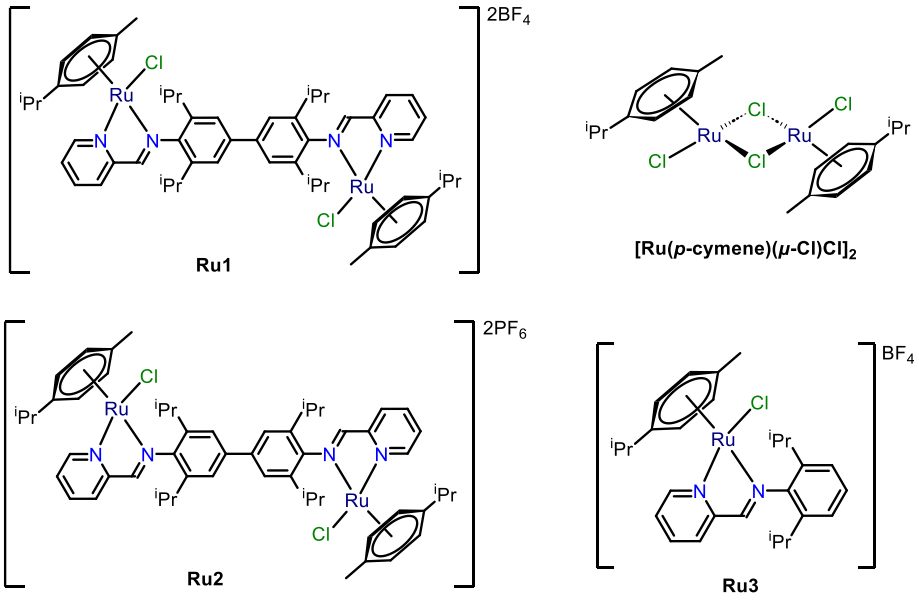

Figure 5. Bimetallic and monometallic catalysts are employed in the present study for quinoline synthesis.

Moving beyond these variations, we have also explored the reaction using different aliphatic alcohols. Acyclic aliphatic alcohols such as ethanol, 2-butanol, 2-heptanol and 2-octanol, yielding the desired products **3i** (83%), **3j** (81%), **3k** (83%) and **3l** (80%) in high yields. The studies have been further extended to include cyclic alcohol substrates such as cyclopentanol, cyclohexanol, and cycloheptanol, leading to the formation of the desired quinoline **3m**, **3n**, and **3o**, in 83, 89, and 78%, respectively.

Scheme 3. Substrate scope for the coupling of 2-nitrobenzyl alcohol with secondary alcohols.

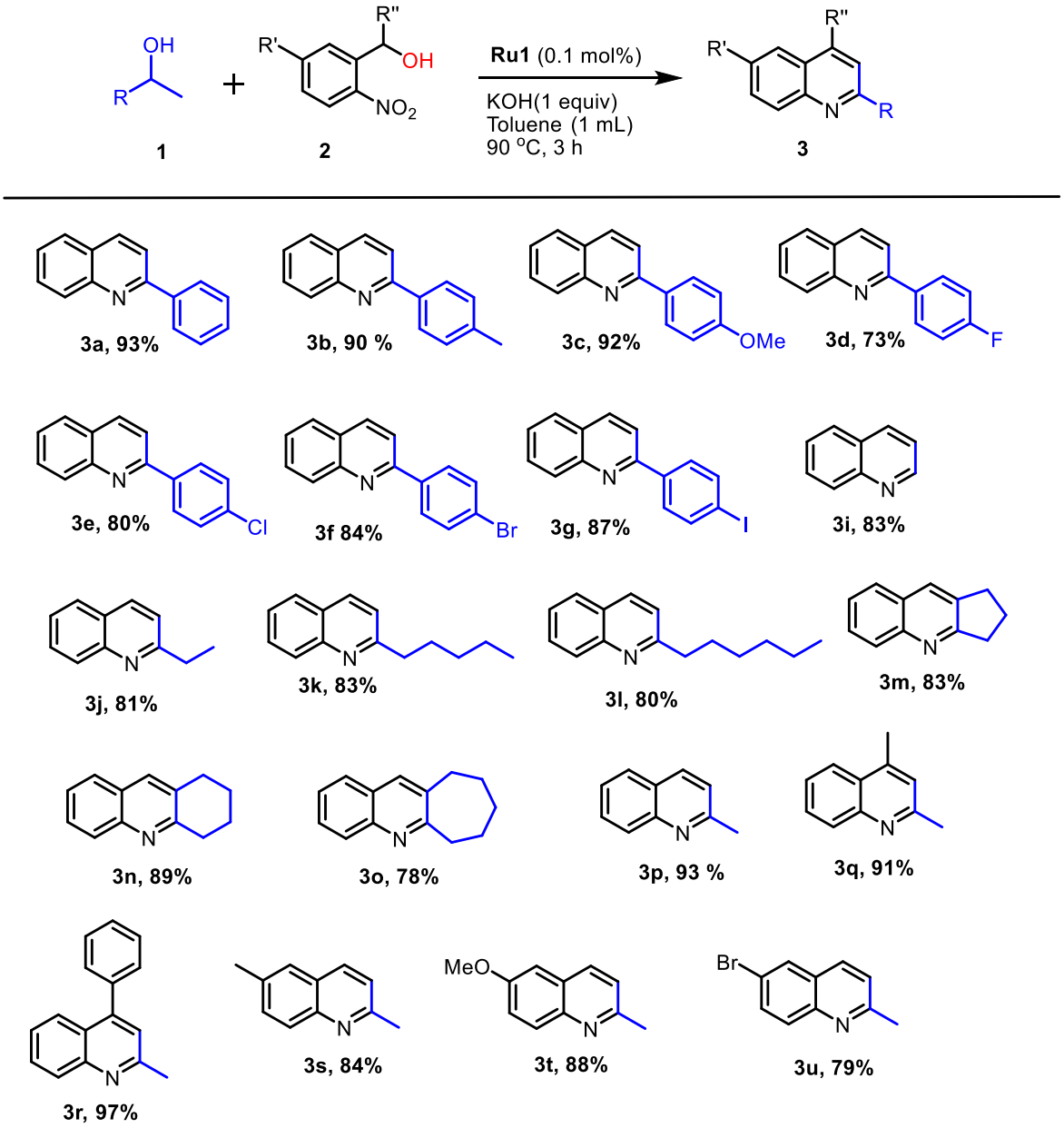

Reaction conditions: 2-nitrobenzylacohol (1 mmol), secondary alcohol (2 mmol), **Ru1** (0.1 mol%), toluene (1 mL), KOH (1 equiv.), 90 °C for 3 hours, isolated yield.

Remarkably, among various aliphatic secondary alcohols, isopropanol exhibited superior reactivity, resulting in the synthesis of **3p** with an impressive yield of 93%. This intriguing observation prompted additional investigations to confirm its efficiency. Subsequent reactions conducted in isopropanol, using (2-nitrophenyl)(phenyl)methanol under optimized conditions, led to the formation of **3q** in 91% yield. Similarly, the reaction of 2-nitrobenzophenone with isopropanol afforded **3r** in a substantial yield of 97%.

Furthermore, the substrate scope for 2-nitrobenzyl alcohol has also been explored with respect to an electron-donating (methyl or methoxy) substituent positioned para to the nitro group, yielding quinolines **3s** and **3t** in 84 and 88% yield, respectively. Contrastingly, electron-withdrawing bromo-substituted 2-nitrobenzyl alcohol, decreased the yield of **3u** to 79%. The increased reactivity of isopropanol within the catalytic system is very significant due to its efficient deprotonation by KOH, which improves the overall efficiency of the reaction process.

Scheme 4. Substrate scope for the coupling of 2-aminobenzyl alcohol with secondary alcohols.

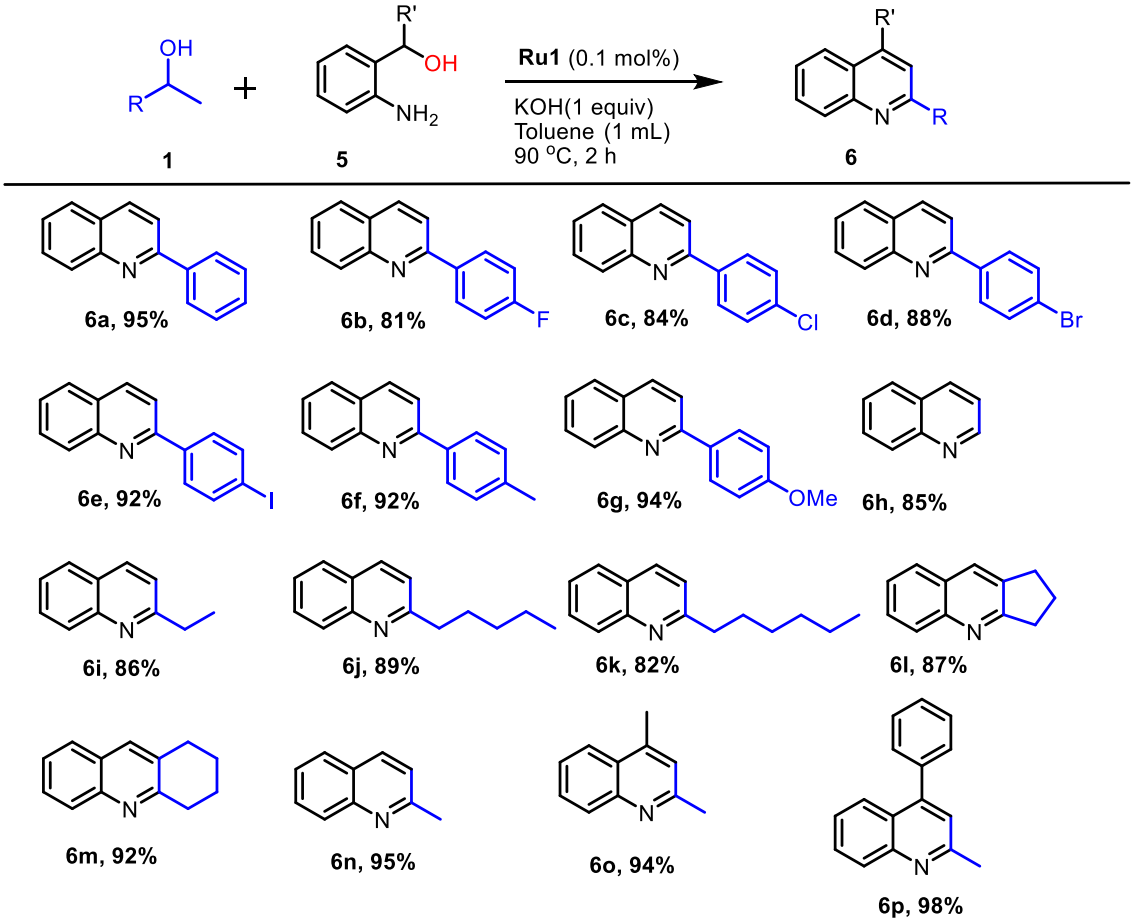

Reaction conditions: 2-aminobenzylacohol (1 mmol), secondary alcohol (1 mmol), **Ru1** (0.1 mol%), toluene (1 mL), KOH (1 equiv.), 90 °C for 2 hours, isolated yield.

Subsequently, the reaction of 2-aminobenzyl alcohol (**5a**) and 1-phenylethanol (**1a**), was investigated using **Ru1** as a catalyst. Optimal results were achieved when KOH was used as a base at 90°C in toluene for a duration of 2 hours with 0.1 mol% of **Ru1** yielding **6a** with 95% yield. Further studies incorporated the reaction between derivatives of 1-phenylethanol with 2-aminobenzyl alcohol (Scheme 4). Electron-withdrawing substituents, such as fluorine led to a relatively lowered yield of the desired product **6b** (81%). On the other hand, substituents such as chlorine, bromine, and iodine yielded **6c**, **6d**, and **6e** in 84, 88 and 92% respectively. Remarkably, 1-phenylethanol derivatives with strong electron-donating substituents resulted in 92 and 94% yield of **6f** and **6g**. To further expand the substrate scope, aliphatic acyclic and cyclic alcohols were also investigated, resulting in the formation of desired products **6h-6m** in good yields ranging from 85 to 89%. Here again high reactivity of isopropanol has been observed to produce **6n**, **6o** and **6p** in 95, 94 and 98% yield, respectively.

Functionalization of Steroids

To showcase the adaptability and significance of our catalytic approach, we extended its application to the late-stage functionalization of bioactive steroids including estradiol, cholesterol, and tetralol derivatives.[56,57] These steroids have been well studied for their therapeutic applications through derivatization and structure-activity studies. Prominently, molecules like progesterone and estradiol have found widespread use in hormone replacement therapy. Cholesterol-derived quinolines have been demonstrated for their function in reversing protein aggregation processes, resulting in the discovery of new drugs.[58–61] Tetralol derivatives show potential in treating social anxiety, premenstrual dysphoric disorder, post-traumatic stress disorder and obsessive-compulsive disorder.[62,63]

Under optimal reaction conditions, the reaction between 2-nitrobenzyl alcohol and tetralol derivatives (**7a** and **7b**) afforded desired **8a** and **8b** quinolines in 91 and 88% yield, respectively (Scheme 5).

Scheme 5. Coupling of 2-nitrobenzyl alcohol with tetralol derivatives.

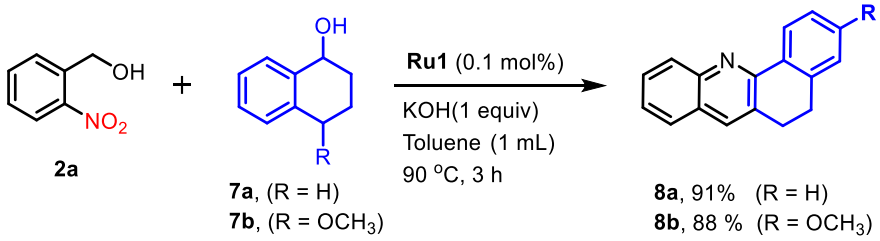

When the same reaction was performed with cholesterol under optimal reaction conditions at 90 °C using **Ru1**, quinoline formation was poor, yielding only trace amounts of **10a** (Scheme 6). The reaction efficiency, however, significantly improved by increasing the temperature to 120 °C and extending duration of the reaction to 5 h, to produce the desired quinoline **10a** in 72% yield. Similarly, estradiol (**11a**) and pregnenolone (**13a**) reacted effectively with 2**a** under similar reaction conditions (120 °C; 4 h) to yield quinolines **12a** and **14a** in 81 and 69%, respectively. This underscores the broad applicability of the bimetallic **Ru1**-based catalytic approach and its significance in simplifying the synthesis of important molecules of pharmaceutical impact (Figure S19-S24 for HRMS).

Scheme 6. Late-stage functionalization of steroids with 2-nitrobenzyl alcohol

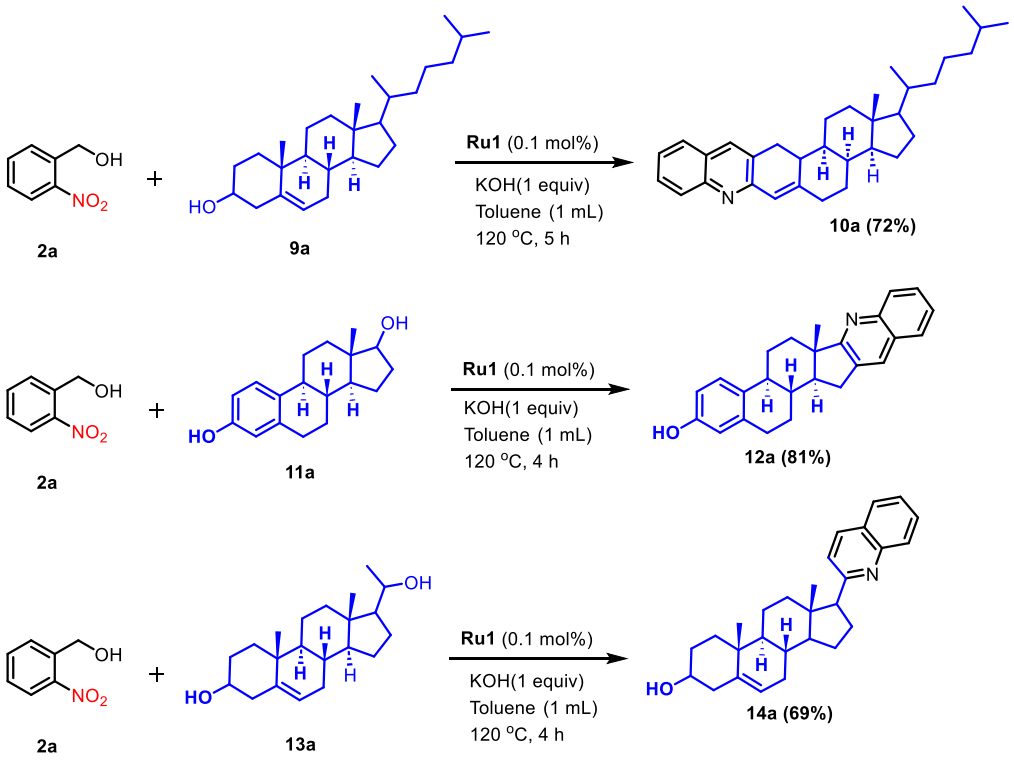

Reaction conditions: 2-nitrobenzylacohol (0.25 mmol), steroid derivatives (0.50 mmol), **Ru1** (0.1 mol%), toluene (1 mL), KOH (1 equiv.), 120 °C for 4 or 5 hours, isolated yield.

Catalytic efficiency of Ru1 for quinoline synthesis

The efficiency of catalyst **Ru1** is revealed in terms of TON and TOF calculated for the model reaction of 2-nitrobenzyl alcohol with 1-phenylethanol under optimized conditions. Thus, for 0.1 mol% of the catalyst loading, the observed TON and TOF were 930 and 310 h^{-1}. Reduction of catalyst loading to 0.01 mol% leads to an almost 9-fold increase in both TON and TOF (8200 and 2733 h^{-1}, respectively). The highest TON and TOF of 6.7×10^3 and 2.3×10^3

h^{-1}, respectively, were observed when the catalyst loading was further lowered down to 0.001 mol%, although selectivity for quinoline formation decreased (Table 1, entry 18) (also see Table S1 for a comparison of the reaction parameters of the present system with that of earlier reported effective catalysts). It is also important to highlight here that the present system **Ru1** can be used in scale-up reactions, as has demonstrated by the success in case of the bioactive quinoline steroid and in the case of 2-methylquinoline scale-up reaction (Scheme 7). For example, the reaction of 5 mmol of 2-nitrobenzyl alcohol with 11 mmol tetralol under optimized reaction conditions, using 0.1 mol% catalyst, produced the corresponding quinoline in 87% yield (1.02 g), further attesting the applicability of **Ru1** for scale up reactions.

Scheme 7. Scale-up reaction with 2-nitrobenzyl alcohol.

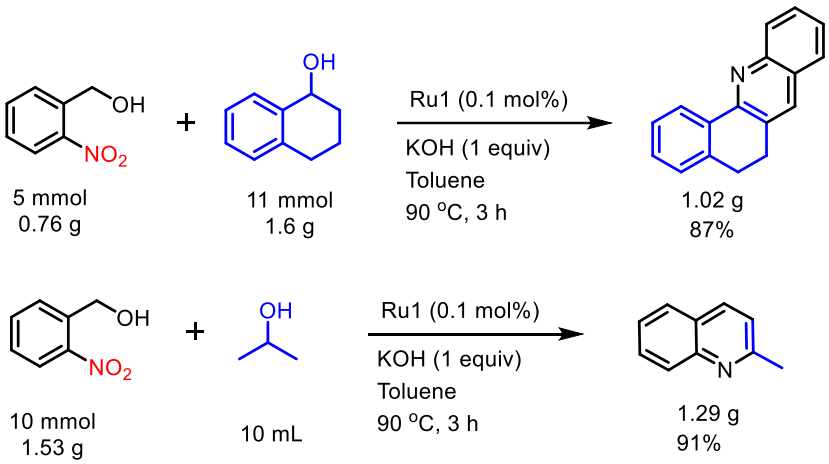

Mechanistic Insights

Several control experiments were conducted to gain a better understanding of the mechanism involved in the formation of quinoline from the reaction between **1a** and **2a** (Scheme 8). Initially, the reaction was performed in the absence of a base or catalyst to ascertain their roles. It was observed that the reaction did not proceed in the absence of either base or catalyst (Scheme 8a and b). Then, the reaction was carried out between **1a** and **2a** and 30 minutes after the start of the reaction, GC-MS analysis revealed the presence of acetophenone and 2-amino-benzaldehyde as intermediates (Scheme 8c and Figure S16). This result suggests that the mechanism involves the dehydrogenation of alcohol a followed by hydrogenation of nitro to amine and subsequent condensation reactions to produce a desired product.

The significance of alcohol dehydrogenation and the formation of an intermediate has been firmly established through a series of control experiments. Initially, when the reaction

was conducted between 2-nitrobenzyl alcohol and acetophenone (as one of the intermediate species), yielding only trace amount of **3a** (Scheme 8, d). This result signifies the pivotal role of alcohol dehydrogenation, as it paves the way for the conversion of the starting materials into the desired product. To support the result, a subsequent reaction involving 1-phenylethanol and 2-aminobenzaldehyde yielded **3a** with a 69% yield (Scheme 8, e). This result effectively reiterates the importance of dehydrogenation as an important intermediate step leading to the eventual formation of **3a**.

Scheme 8. Control experiments for mechanistic insights

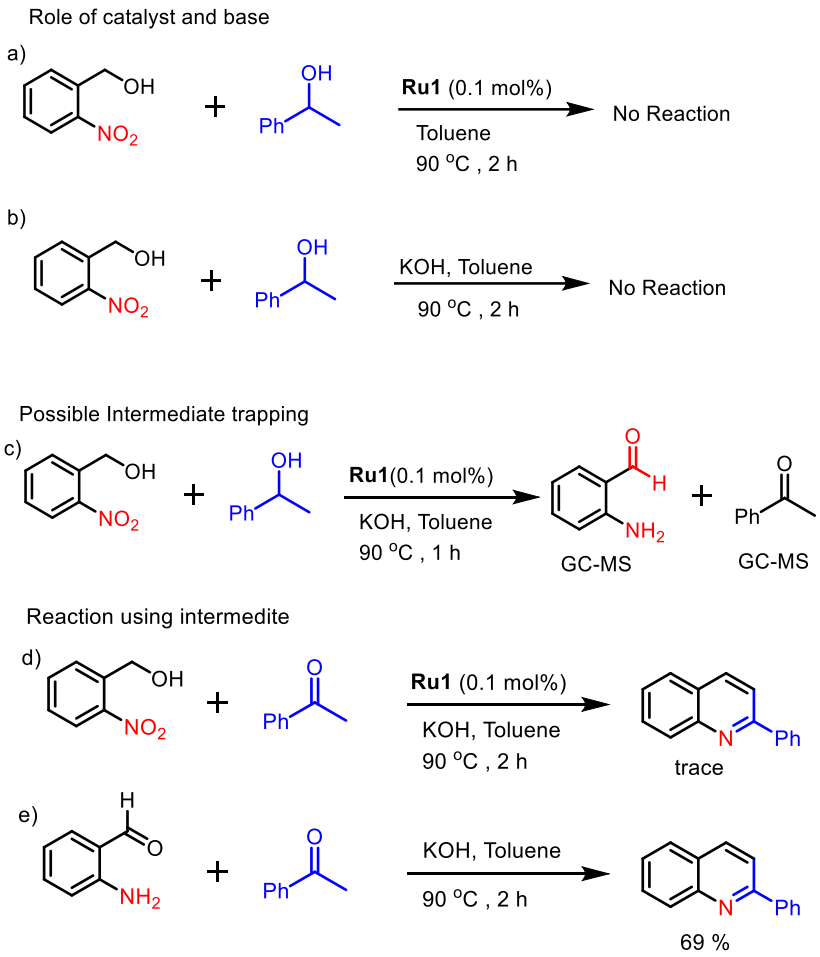

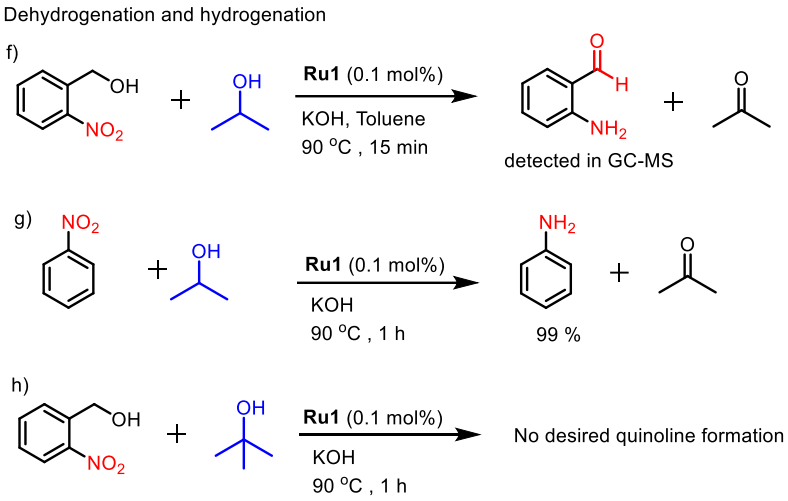

In a parallel experiment, where 2-nitrobenzyl alcohol was reacted with isopropanol, an initial formation of 2-aminobenzaldehyde occurred within 30 minutes (Scheme 8, f and Figure S17). Over the course of an hour, this intermediate species then converted into 2-methylquinoline. These observations provide compelling support for the hypothesis that 2-aminobenzaldehyde intermediate formed from the alcohol dehydrogenation step.

Under optimized conditions, the reaction of nitrobenzene in isopropanol produced aniline in 99 % yield (Scheme 8, g). The reaction involving 2-nitrobenzyl alcohol and tert-butyl alcohol was conducted under standard conditions but failed to yield the desired product (Scheme 8, h). This result provides strong evidence for the crucial role of an alpha proton on the alcohol for dehydrogenation, revealing a significant aspect of the reaction mechanism.

Finally, an in-situ React IR experiment was carried out to glean more information about the progress of the reaction and to track the functional group transformations during the course of the reaction. The IR probe was inserted into the reactor through an adapter at 60 ^{o}C (as opposed to the optimized reaction temperature of 90 ^{o}C, see Table 1) (Figure S11-S12). The results obtained are pictorially summarized in Figure 5. The nitro groups stretching vibration (at 1350 and 1460 cm^{-1}) were disappear and appearance of C-N stretching at 1288 cm^{-1} of -NH_2 group with the progress of reaction has been seen in IR spectra. An increase in the intensity of the band appearing at 1690 cm^{-1} has been identified as the C=O stretching vibration of the ketone intermediate. As the progress of reaction intensity of the peak at 1690 cm^{-1} disappear (along with disappearance of -NH_2 group at 1288 cm^{-1}) and the appearance of C=N stretching vibration of quinoline at1660 cm^{-1} is indicating the formation of quinoline. This suggested that the intermediate carbonyl and amino was generated initially and consumed gradually in the reaction system (Figure 6).

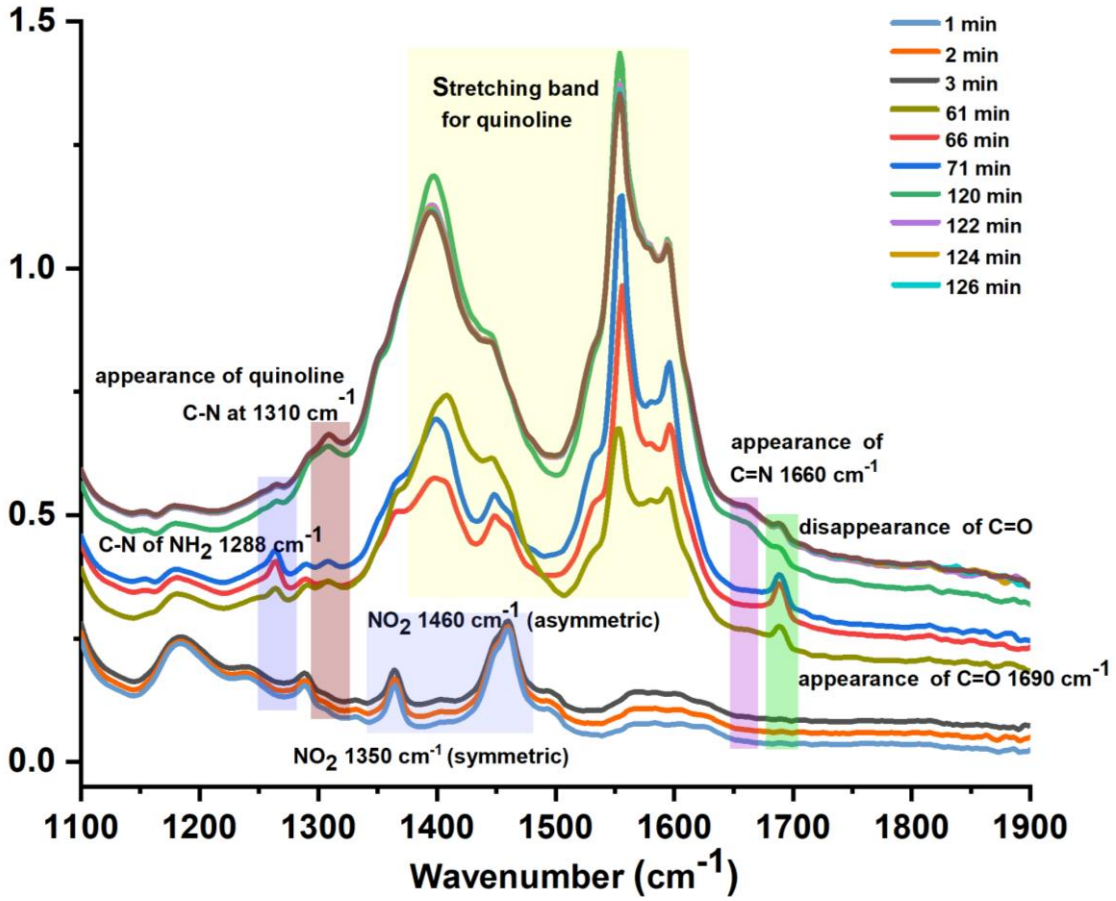

Figure 6. Selected FT-IR spectra of the react IR experiments.

Based on the evidence gathered from the control experiments described above and from the knowledge available from literature,[24,26,64] we propose the catalytic cycle shown in Figure 6 in two parts (Part A and Part B) for the transformation of 2-nitrobenzyl alcohol to quinolines. In the first step of the catalysis (Part A), the chloride linkage of the catalyst LnRu-Cl (**Ru1**) is replaced by alkoxide species (**LnRu-OCH(CH$_3$)Ph**), aided by the presence of base KOH. This alkoxo-coordinated ruthenium intermediate has been seen in the mass spectrometry through the peak appearing for $[M+2BF_4+ K]^+$ at *m/z* 1456.588, during the initial phase of the reaction (Figure S13 and S15). In the next step, Ru-alkoxide **LnRu-OCH(CH$_3$)Ph** undergoes β-hydride elimination, resulting in the release of acetophenone and ruthenium hydride species **LnRu-H**, whose molecular ion appears in the ESI-MS at *m/z* 1151.264 correspond to $[M+BF_4+Na+K-H]^+$ (Figure 7 and S14). H_2O produced in the initial stages of the reaction converts this hydride complex to the corresponding hydroxide species **LnRu-OH**, which then combines with 2-nitrobenzyl alcohol to produce **LnRu-OCH$_2$Ar**. This is followed by the dehydrogenation of benzyl alcohol via β-hydride elimination to release 2-nitrobenzaldehyde to the system and regenerate the ruthenium hydride species **LnRu-H**. Thus, Part A of the mechanism produces 4

equivalents of molecular hydrogen through two dehydrogenation reactions involving both primary and secondary alkoxides coordinated to Ru centers. In Part B of the mechanism, three out of these four equivalents of hydrogen produced are consumed to convert one equivalent of 2-nitro benzaldehyde to 2-amino benzaldehyde. The remaining one equivalent of hydrogen would be used up to reduce a further equivalent of nitro benzaldehyde after every three cycles. However, the use of more than two equivalents of 2-phenyl ethanol per equivalent of nitro benzyl alcohol ensures enough hydrogen production at the end of each cycle so that the reaction rate is not impeded. The final step of the mechanism involves a base-catalyzed aldol condensation of 2-aminobenzaldehyde with acetophenone, followed by dehydrative cyclization to provide the desired quinoline (also see ESI Scheme S1).

This above mechanism can also be extrapolated to understand the lower efficiency obtained for the mononuclear catalyst **Ru3** (Table 2 and Figure S18), which produces only two equivalents of H_2 at the end of each cycle while the reduction of 2-nitrobezaldehyde requires three equivalents of hydrogen. This essentially means that the catalysis has to run three full cycles to reduce two equivalents of 2-nitrobezaldehyde, while the same number three catalytic cycles with **Ru1** would produce twelve equivalents of hydrogen that is sufficient to reduce four equivalents of 2-nitrobezaldehyde. This clearly demonstrates that superiority of binuclear complex over its monometallic version for the quinoline synthesis.

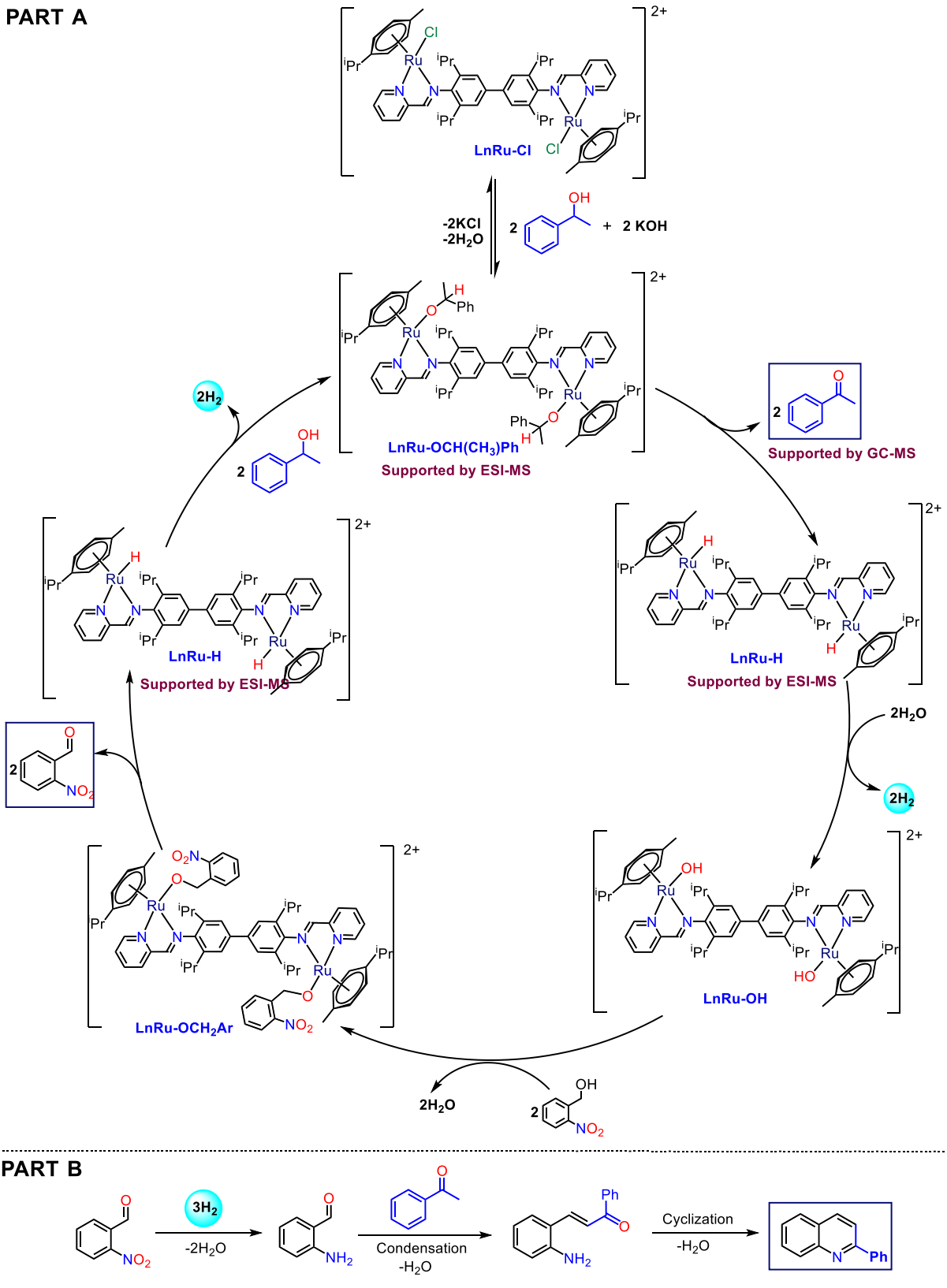

Figure 6. Plausible reaction mechanism for quinoline synthesis using **Ru1** catalyst (see text for a full description of the mechanism).

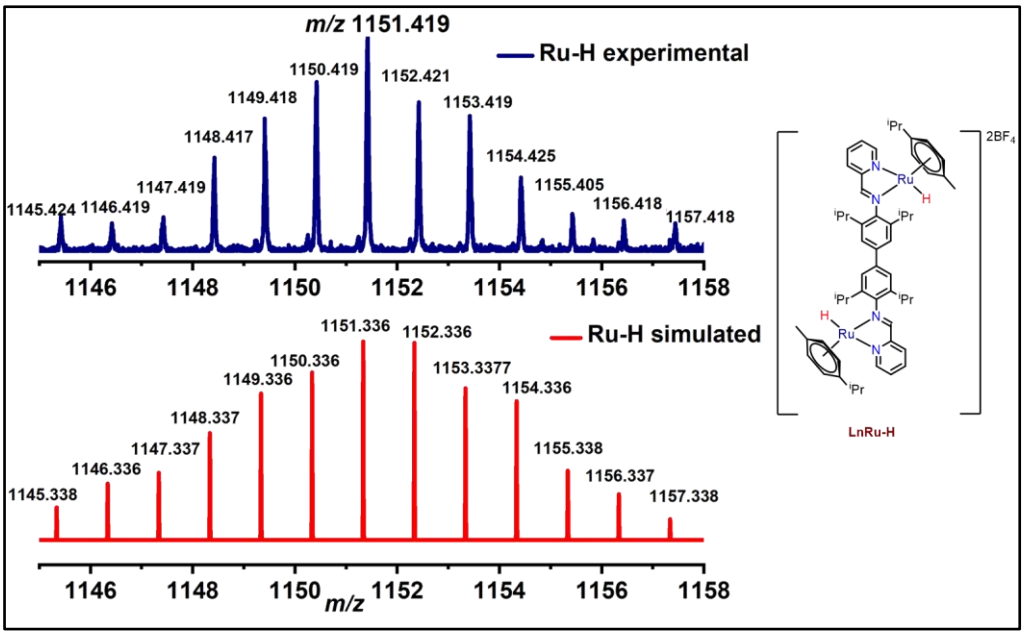

Figure 7. ESI-MS spectra showing the experimental and simulated isotopic patterns of $[M+BF_4+Na+K-H]^+$ ion peak at *m/z* 1151.264 for Ru-hydride intermediate in methanol.

Conclusions

The present work demonstrates that **Ru1** is an efficient catalyst for the synthesis of quinolines directly starting from 2-nitrobenzyl alcohol and a secondary alcohol in the presence of a base. The broad applicability of this catalytic approach for a large variety of substrates, including its versatility for modifying bioactive steroids affording a remarkable yield of quinoline derivatives, makes this a unique catalytic system. Even when employed in small quantities (0.1 mol%), the catalyst orchestrated the desired transformation with remarkable efficiency. Further lowering of the catalyst loading to 0.001 mol%, leads to the highest observed TON and TOF of 67000 and 22333 h^{-1}, respectively, underscoring the catalyst's unparalleled activity even under such low loading. Notably, the present catalytic approach eliminates the need for high pressure H_2 or harsh reaction conditions such as elevated temperature (120-160 °C), longer reaction duration (18-48 hours), and high catalyst loading (1.5-5 mol%). Additionally, this methodology neither requires moisture-sensitive phosphine ligands (Table S1) nor generates any waste that is harmful to the environment.

The proposed mechanism for the catalytic cycle has been supported and substantiated by spectroscopic techniques including React IR experiments. The postulated mechanism also explains the superiority of the bimetallic catalyst **Ru1** vis-à-vis the monometallic **Ru3**, in terms

of the number of equivalents of hydrogen produced that is necessary for the reduction of nitro-benzaldehyde to the corresponding amino compound at the end of each catalyst cycle.

Experimental section

Materials and methods

All the experiments were carried out in a well-ventilated fume hood. The starting materials such as 2,2′,6,6′-tetraisopropylbenzidine (TIBZ), Schiff base ligands $\mathbf{L^1}$ and $\mathbf{L^2}$, 4-Bromo-2,6-diisopropylaniline, and [Ru(*p*-cymene)(μ-Cl)Cl]$_2$ were prepared according to the reported procedures.[50,52,53] Ruthenium(III)trichloride trihydrate, α-phellandrene, pyridine-2-carbaldehyde (Sigma Aldrich), bromine (Spectrochem), 2,6-diisopropylaniline (Alfa Aesar), 2-nitrobenzyl alcohol (Spectrochem), and 2-amino benzyl alcohol (Spectrochem) were used as received. Other substrates and analytical grade solvents were procured commercially and used without any further purification. The ruthenium compounds reported herein are air and moisture stable and hence all manipulations were carried out under normal atmosphere.

Physical measurements and instruments

^{1}H and ^{13}C NMR spectra were recorded on a Bruker AV III 400 MHz NMR spectrometer in $CDCl_3$ or DMSO-d_6. Melting points were measured in glass capillaries and are reported uncorrected. FT-IR spectra were recorded on a PerkinElmer Spectrum One Infrared Spectrometer (Model number 73465) as KBr diluted discs in the frequency range 4000–400 cm^{-1}. Elemental analyses were performed on a Thermo Finnigan (FLASH EA 1112) microanalyzer. ESI-MS measurements were performed on a Bruker Maxis Impact electrospray mass spectrometer. UV-NIR-3600 spectrophotometer from Shimadzu was used for the UV-visible studies. Powder X-ray diffraction studies were recorded on a Rigaku SmartLab powder X-ray diffractometer using Cu-Kα radiation (λ= 1.54190 Å). Molecular structures of **Ru1** and **Ru3** were determined using Mo-Kα radiation (λ = 0.71073 Å) on a Bruker D8 QUEST diffractometer.[65-68] Mettler Toledo ReactIR 700 instrument was used to perform in-situ react IR experiments. An Agilent 7890A GC system with an FID detector and a J & W DB-1 column (10 m, 0.1 mm ID) was used to conduct GC-MS analysis.

Synthesis of [{(*p*-cymene)$_2$(RuCl)$_2$L^1}·2BF$_4$] (Ru1)

Schiff base ligand $\mathbf{L^1}$ (105 mg, 0.2 mmol)) and [Ru(*p*-cymene)(μ-Cl)Cl]$_2$ (122 mg, 0.2 mmol) were dissolved together in ethanol (50 mL) in a 100 mL round bottom flask. After

stirring for a few minutes, two equivalents of sodium tetrafluoroborate (44 mg, 0.4 mmol) was added to the reaction mixture followed by vigorous stirring at room temperature for a period of 12 h. The color of the reaction mixture changed from light brown to dark red during the course of reaction. After removal of the solvent under vacuum, crude **Ru1** was obtained as dark residue in high yield. The residue was dissolved in dichloromethane. Addition of diethyl ether to this solution resulted in a yellow color precipitate. This precipitate on recrystallization from ethanol:acetone (4:1 v/v) afforded the product as dark-red blocks. Yield: 193 mg (78%) Mp. >250 °C. Anal. Cal for $C_{56}H_{70}Cl_2N_4Ru_2B_2F_8$**;** C, 53.90; H, 5.62; N, 4.51. Found: C, 53.33; H, 6.03; N, 4.13; ESI-MS: Calcd. for $C_{56}H_{70}Cl_2N_4Ru_2BF_4$, $[M-BF_4]^+$: 1159.3112 Found: 1159.3119; ^{1}H NMR (400 MHz, DMSO-d_6) δ 9.70 (d, $^3J_{H,H}$ = 5.9 Hz 2H), 9.04 (s, 2H), 8.35-834 (m, 4H), 7.97-7.96 (m, 4H), 7.76 (s, 2H), 7.67 (s, 2H), 6.13(d, $^3J_{H,H}$ = 6.4 Hz, 2H), 5.68 (d, $^3J_{H,H}$ = 6.4 Hz, 2H), 5.49 (d, $^3J_{H,H}$ = 6.5 Hz, 2H), 5.37 (d, $^3J_{H,H}$ = 6.5 Hz, 2H), 3.81 (sept, $^3J_{H,H}$ = 6.4 Hz, 2H), 2.65 (sept, $^3J_{H,H}$ = 6.3 Hz, 4H), 2.16 (s, 6H), 1.56 (d, $^3J_{H,H}$ = 6.2 Hz, 6H), 1.38 (d, $^3J_{H,H}$ = 6.3 Hz 6H), 1.24 (d, $^3J_{H,H}$ = 6.3 Hz, 6H), 1.07 (d, $^3J_{H,H}$ = 6.3 Hz, 12H), 1.05 (d, $^3J_{H,H}$ = 6.2 Hz, 6H) *ppm*. ^{13}C NMR (101 MHz, DMSO-d_6): δ173.01, 156.94, 154.45, 148.55, 142.68,141.02, 140.64, 130.63, 130.16, 123.41, 105.40, 101.89, 87.58, 86.68, 86.47, 85.02, 31.02, 28.51, 28.01, 27.01, 26.21, 23.67, 22.72, 22.09, 21.96, 18.95 *ppm*. FT-IR (KBr pellet, cm^{-1}) 2958, 1630, 1469, 1436, 1182, 968, 695; UV-Vis (dichloromethane, λ_{max} (nm), ε ($\times 10^5$ M^{-1} cm^{-1})) 277 (1.3), 373 (0.3).

Synthesis of [{*p*-cymene)$_2$(RuCl)$_2$L^1}·2PF$_6$] (Ru2)

Schiff base ligand **L^1** (105 mg, 0.2 mmol)) and [Ru(*p*-cymene)(μ-Cl)Cl]$_2$ (122 mg , 0.2 mmol) were dissolved together in ethanol (50 mL) in a 100 mL round bottom flask and stirred for a few minutes after which two equivalents of ammonium hexafluorophosphate (0.4 mmol, 66 mg) was added and stirred at room temperature for an additional period of 12 h. The color of the reaction mixture changed from light brown to yellow during the reaction. After removal of the solvent under vacuum yielded crude **Ru2** which was dissolved in dichloromethane. Addition of diethyl ether to this solution resulted in a red color precipitate of analytically pure **Ru2**. Yield: 202 mg (83%) Mp. >250 °C. Anal. Cal for $C_{56}H_{70}Cl_2N_4Ru_2P_2F_{12}$**;** C, 49.38; H, 5.18; N, 4.11. Found: C, 49.06; H, 5.11; N, 4.03; ESI-MS: Calcd. for $C_{56}H_{70}Cl_2N_4Ru_2PF_6$, $[M-PF_6]^+$: 1217.2718 Found: 1217.2525; ^{1}H NMR (400 MHz, DMSO-d_6) δ 9.73 (d, $^3J_{H,H}$= 5.5 Hz 2H), 9.06 (s, 2H), 8.38-8.35 (m, 4H), 8.10-8.01 (m, 4H), 7.98-7.70 (m, 2H), 7.79 (s, 2H), 7.71 (s, 2H), 6.16 (d, $^3J_{H,H}$= 6.3 Hz, 2H), 5.72 (d, $^3J_{H,H}$= 6.3 Hz, 2H), 5.53 (d, $^3J_{H,H}$= 6.3

Hz, 2H), 5.40 (d, $^{3}J_{H,H}$= 6.3 Hz, 2H), 3.85 (sept, $^{3}J_{H,H}$= 6.5 Hz, 2H), 2.69 (sept, $^{3}J_{H,H}$= 6.3 Hz, 4H), 2.19 (s, 6H), 1.58 (d, $^{3}J_{H,H}$= 6.6 Hz, 6H), 1.41 (d, $^{3}J_{H,H}$= 6.3 Hz 6H), 1.27 (d, $^{3}J_{H,H}$= 6.7 Hz, 6H), 1.07 (d, $^{3}J_{H,H}$= 6.6 Hz, 12H), 0.95 (d, $^{3}J_{H,H}$= 6.6 Hz, 6H) *ppm*. ^{13}C NMR (101 MHz, DMSO-d_6) δ 173.50,156.43, 153.95, 148.04, 142.17,140.51, 140.13, 130.18, 129.66, 122.90, 105.90, 101.38, 87.07, 86.17, 85.96, 84.51, 30.51, 28.01, 27.50, 26.50, 25.70, 23.17, 22.21, 21.58, 21.46, 18.08 *ppm*. FT-IR (KBr pellet, cm^{-1}) 3013, 1631, 1483, 1252, 1097, 844, 556; UV-Vis (dichloromethane, λ_{max} (nm), ε ($\times 10^5$ M^{-1} cm^{-1})) 280 (4.0), 378 (1.0).

Synthesis of [{*p*-cymene)$_2$(RuCl)$_2$L^2}·BF$_4$] (Ru3)

Schiff base ligand **L^2** (106 mg, 0.4 mmol)) and [Ru(*p*-cymene)(μ-Cl)Cl]$_2$ (122 mg , 0.2 mmol) were dissolved together in ethanol (50 mL) in a 100 mL round bottom flask under stirring. Two equivalents of sodium tetrafluoroborate (44 mg, 0.4 mmol) was added to this reaction mixture and stirred at room temperature for an additional period of 12 h. The color of the reaction mixture changed from light brown to dark red during the course of the reaction. After removal of the solvent under vacuum, crude **Ru3** was obtained as a yellow residue in high yield. This residue was dissolved in dichloromethane, followed by the addition of diethyl ether to result in a yellow precipitate which on recrystallization from ethanol: dichloromethane (10:1 v/v) afforded **Ru3** as dark red crystals. Yield: 189 mg (88 %) Mp. >250 °C. Anal. Cal for $C_{28}H_{36}ClN_2RuBF_4$**,** C, 53.90; H, 5.82; N, 4.49. Found: C, 54.48; H, 5.57; N, 4.43; ESI-MS: Calcd. for $C_{28}H_{36}ClN_2Ru$, $[M-BF_4]^+$: 537.1609 Found: 537.1562; ^{1}H NMR (400 MHz, DMSO-d_6) δ 9.69 (d, $^{3}J_{H,H}$ = 5.2 Hz 1H), 9.01 (s, 1H), 8.34-8.31 (m, 2H), 7.96-94 (m, 1H), 7.52-7.50(m, 2H), 7.42-7.41 (m, 1H), 6.03 (d, $^{3}J_{H,H}$ = 5.9 Hz, 1H), 5.65 (d, $^{3}J_{H,H}$ = 6.1 Hz, 1H), 5.49 (d, $^{3}J_{H,H}$ = 5.9 Hz, 1H), 5.33 (d, $^{3}J_{H,H}$ = 6.1 Hz, 1H), 3.74 (sept, $^{3}J_{H,H}$ = 6.9 Hz, 1H), 2.59 (sept, $^{3}J_{H,H}$ = 6.6 Hz, 2H), 2.13 (s, 3H), 1.45 (d, $^{3}J_{H,H}$ = 6.6 Hz, 3H), 1.26 (d, $^{3}J_{H,H}$ = 6.7 Hz 3H), 1.14 (d, $^{3}J_{H,H}$ = 6.8 Hz, 3H), 1.05 (d, $^{3}J_{H,H}$ = 6.9 Hz, 6H), 0.09 (d, $^{3}J_{H,H}$ = 6.5 Hz, 3H) *ppm*. ^{13}C NMR (101 MHz, DMSO-d_6) δ 173.80, 156.78 154.36, 148.62, 141.64, 140.94, 140.04, 130.39, 130.04, 124.94, 105.01, 101.61, 87.35, 86.48, 85.20, 30.82, 28.15, 27.65, 27.04, 26.21, 23.57, 22.70, 22.08, 21.76, 18.41 *ppm*. FT-IR (KBr pellet, cm^{-1}) 2966, 1636, 1470, 1670, 772, 549; UV-Vis (dichloromethane, λ_{max} (nm), ε ($\times 10^5$ M^{-1} cm^{-1})) 259 (7.1), 326 (2.4).

General procedure for the synthesis of quinolines from 2-nitrobenzyl alcohol

An oven-dried round bottom flask containing a stir bar was charged with **Ru1** (0.1 mol%), potassium hydroxide (112 mg, 2 mmol), 2-nitrobenzyl alcohol (154 mg, 1 mmol), and

excess of secondary alcohol (>2 mmol) in toluene (1 mL) and was stirred at 90 °C for 3 hours. GC-MS analysis was used to monitor the product formation. After completion of the reaction, the resulting mixture was concentrated under reduced pressure and the residue was purified by column chromatography using petroleum ether / ethyl acetate mixture (95:5) as the eluent. The pure product was analyzed by NMR spectroscopy (details in ESI).

General procedure for the synthesis of quinolines from 2-amino benzyl alcohol

An oven-dried round bottom flask containing a stir bar was charged with **Ru1** (0.05 mol%), potassium hydroxide (56 mg, 1 mmol), 2-aminobenzyl alcohol (124 mg, 1 mmol), and secondary alcohol (1 mmol) in toluene (1 mL) and was stirred at 90 °C for 2 hours. GC-MS analysis was used to track the product formation. After completion of the reaction, the resulting mixture was concentrated under reduced pressure and the residue was purified by column chromatography using petroleum ether / ethyl acetate mixture (95:5) as the eluent. The pure product was analyzed using NMR spectroscopy.

General procedure for scale-up reaction

An oven-dried round bottom flask containing a stir bar has been charged with **Ru1** (0.1 mol%), potassium hydroxide, 2-nitrobenzyl alcohol (0.76 g, 5 mmol), and tetralol (1.6 g, 11 mmol) in toluene (5 mL) and was stirred at 90 °C for 3.5 hours. GC-MS analysis was used to monitor the reaction. After completion of the reaction, the resulting mixture was concentrated under reduced pressure. The residue obtained was purified by column chromatography using petroleum ether / ethyl acetate mixture (95:5) as the eluent. The pure product was analyzed using NMR spectroscopy. Yield for gram scale reaction 1.02 g (87%) and yield of 1 mmol scale reaction 211 mg; (91%).

ASSOCIATED CONTENT

Supporting Information. The Supporting Information is available: Crystallographic details, spectral characterization and additional figures and tables.

Crystallographic information of the **Ru1** and **Ru3**. CCDC numbers of **Ru1**-2299728 and **Ru3**-2299729 contain the supplementary crystallographic data for this paper.

AUTHOR INFORMATION

Corresponding Authors

Ramaswamy Murugavel - Department of Chemistry, Indian Institute of Technology Bombay, Powai, Mumbai-400076, India. *ORCID: orcid.org/0000-0002-1816-3225*.

E-mail: rmv@chem.iitb.ac.in

Authors

Gopal Deshmukh - Department of Chemistry, Indian Institute of Technology Bombay, Powai, Mumbai-400076, India. *ORCID: orcid.org/0009-0008-1169-7460*.

Santosh J. Gharpure - Department of Chemistry, Indian Institute of Technology Bombay, Powai, Mumbai-400076, India. *ORCID: orcid.org/0000-0002-6653-7236*.

Conflicts of interest

There are no conflicts to declare.

Acknowledgements

This work was supported by SERB, New Delhi through a J. C. Bose Fellowship grant to R. M. (SB/S2/JCB-85/2014). G.D. thanks CSIR/UGC New Delhi and IIT Bombay for a research fellowship. The authors thank the IoE-funded central facilities and SAIF, IIT Bombay for help with various spectral measurements.

References

(1) Vitaku, E.; Smith, D. T.; Njardarson, J. T. Analysis of the Structural Diversity, Substitution Patterns, and Frequency of Nitrogen Heterocycles among U.S. FDA Approved Pharmaceuticals. *J. Med. Chem.* **2014**, *57*, 10257–10274.

(2) Hu, Y. Q.; Gao, C.; Zhang, S.; Xu, L.; Xu, Z.; Feng, L. S.; Wu, X.; Zhao, F. Quinoline Hybrids and Their Antiplasmodial and Antimalarial Activities. *Eur. J. Med. Chem*, 2017, 139, 22–47.

(3) Sriram, D.; Senthilkumar, P.; Dinakaran, M.; Yogeeswari, P.; China, A.; Nagaraja, V. Antimycobacterial Activities of Novel 1-(Cyclopropyl/Tert-Butyl/4-Fluorophenyl)-1,4-Dihydro-6-Nitro-4-Oxo-7-(Substituted

Secondary Amino)-1,8-Naphthyridine-3-Carboxylic Acid. *J. Med. Chem.* **2007**, *50*, 6232–6239.

(4) Gorka, A. P.; De Dios, A.; Roepe, P. D. Quinoline Drug-Heme Interactions and Implications for Antimalarial Cytostatic versus Cytocidal Activities. *J. Med. Chem.* **2013**, *56*, 5231–5246.

(5) Pony Yu, R.; Hesk, D.; Rivera, N.; Pelczer, I.; Chirik, P. J. Iron-Catalysed Tritiation of Pharmaceuticals. *Nature* **2016**, *529*, 195–199.

(6) Gorka, A. P.; De Dios, A.; Roepe, P. D. Quinoline Drug-Heme Interactions and Implications for Antimalarial Cytostatic versus Cytocidal Activities. *J. Med. Chem.* **2013**, *56*, 5231–5246.

(7) Kaur, K.; Jain, M.; Reddy, R. P.; Jain, R. Quinolines and Structurally Related Heterocycles as Antimalarials. *Eur. J. Med. Chem*. **2010**, 45, 3245–3264.

(8) Strekowski, L.; Gulevich, Y.; Baranowski, T. C.; Parker, A. N.; Kiselyov, A. S.; Lin, S.-Y.; Tanious, F. A.; David Wilson, W. Synthesis and Structure-DNA Binding Relationship Analysis of DNA Triple-Helix Specific Intercalators. *J. Med. Chem.* **1996**, 39, 20, 3980–3983.

(9) Maguire, M. P.; Sheets, K. R.; Mcvety, K.; Spada, A. P.; Zilberstein, A. *A* New Series of PDGF Receptor Tyrosine Kinase Inhibitors: 3-Substituted Quinoline Derivatives. *J. Med. Chem*. **1994**, 37, 2129-2137.

(10) Friedlaender, P. Ueber O-Amidobenzaldehyd. *Berichte der deutschen chemischen Gesellschaft* **1882**, *15*, 2572–2575.

(11) Marco-Contelles, J.; Pérez-Mayoral, E.; Abdelouahid Samadi; Carreiras, M. D. C.; Soriano, E. Recent Advances in the Friedländer Reaction. *Chem. Rev.* **2009**, *109*, 2652–2671.

(12) Mahajan, A.; Chundawat, T. S. Review on the Role of the Metal Catalysts in the Synthesis of Pharmacologically Important Quinoline Substrate. *Mini. Rev. Org. Chem.* **2018**, *16*, 631–652.

(13) Tanwar, B.; Kumar, D.; Kumar, A.; Ansari, M. I.; Qadri, M. M.; Vaja, M. D.; Singh, M.; Chakraborti, A. K. Friedländer Annulation: Scope and Limitations of Metal Salt Lewis Acid Catalysts in Selectivity Control for the Synthesis of Functionalised Quinolines. *New J. Chem.* **2015**, *39* (12), 9824–9833.

(14) Wu, J.; Xia, H. G.; Gao, K. Molecular Iodine: A Highly Efficient Catalyst in the Synthesis of Quinolines via Friedländer Annulation. *Org. Biomol. Chem.* **2006**, *4*, 126–129.

(15) Muchowski, J. M.; Maddox, M. L. Concerning the Mechanism of the Friedländer Quinoline Synthesis. *Can. J. Chem.* **2004**, *82*, 461–478.

(16) Maji, M.; Panja, D.; Borthakur, I.; Kundu, S. Recent Advances in Sustainable Synthesis of N-Heterocycles Following Acceptorless Dehydrogenative Coupling Protocol Using Alcohols. *Org. Chem. Front*. **2021**, 8, 2673–2709.

(17) Sun, K.; Shan, H.; Lu, G. P.; Cai, C.; Beller, M. Synthesis of N-Heterocycles via Oxidant-Free Dehydrocyclization of Alcohols Using Heterogeneous Catalysts. *Angew. Chem., Int. Ed.*, **2021**, 133, 25188–25202.

(18) Corma, A.; Navas, J.; Sabater, M. J. Advances in One-Pot Synthesis through Borrowing Hydrogen Catalysis. *Chem. Rev.* ***2018***, 118, 1410–1459.

(19) Bains, A. K.; Singh, V.; Adhikari, D. Homogeneous Nickel-Catalyzed Sustainable Synthesis of Quinoline and Quinoxaline under Aerobic Conditions. *J.Org. Chem.* **2020**, *85*, 14971–14979.

(20) Mastalir, M.; Glatz, M.; Pittenauer, E.; Allmaier, G.; Kirchner, K. Sustainable Synthesis of Quinolines and Pyrimidines Catalyzed by Manganese PNP Pincer Complexes. *J. Am. Chem. Soc.* **2016**, *138*, 15543–15546.

(21) Goswami, B.; Khatua, M.; Chatterjee, R.; Kamal, N.; Samanta, S. Amine Functionalized Pincer-like Azo-Aromatic Complexes of Cobalt and Their Catalytic Activities in the Synthesis of Quinoline via Acceptorless Dehydrogenation of Alcohols. *Organometallics* **2023**, 42, 1854–1868.

(22) Yu, K.; Chen, Q.; Liu, W. Iron-Catalysed Quinoline Synthesis via Acceptorless Dehydrogenative Coupling. *Org. Chem. Front.* **2022**, *9*, 6573–6578.

(23) Hao, Z.; Zhou, X.; Ma, Z.; Zhang, C.; Han, Z.; Lin, J.; Lu, G. L. Dehydrogenative Synthesis of Quinolines and Quinazolines via Ligand-Free Cobalt-Catalyzed Cyclization of 2-Aminoaryl Alcohols with Ketones or Nitriles. *J. Org. Chem.* **2022**, *87*, 12596–12607.

(24) Bhattacharyya, D.; Adhikari, P.; Deori, K.; Das, A. Ruthenium Pincer Complex Catalyzed Efficient Synthesis of Quinoline, 2-Styrylquinoline and Quinazoline Derivatives via Acceptorless Dehydrogenative Coupling Reactions. *Catal. Sci. Technol.* **2022**, *12*, 5695–5702.

(25) Zhao, H.; Wu, Y.; Ci, C.; Tan, Z.; Yang, J.; Jiang, H.; Dixneuf, P. H.; Zhang, M. Intermolecular Diastereoselective Annulation of Azaarenes into Fused N-Heterocycles by Ru(II) Reductive Catalysis. *Nat. Commun.* **2022**, *13*, 2393-2404.

(26) Chen, X.; Ai, Y.; Liu, D.; Liu, P.; Xu, X.; Yang, J.; Li, F. A Recyclable Covalent Triazine Framework-Supported Iridium(III) Terpyridine Complex for the Acceptorless Dehydrogenative Coupling of o-Aminobenzyl Alcohols with Ketones to Form Quinolines. *Mater. Chem. Front.* **2022**, *6*, 1228–1235.

(27) Zhou, W.; Lei, J. Palladium-Catalyzed Synthesis of Polysubstituted Quinolines from 2-Amino Aromatic Ketones and Alkynes. *Chem. Commun.* **2014**, *50*, 5583–5585.

(28) Cho, C. S.; Ren, W. X. A Recyclable Palladium-Catalyzed Modified Friedländer Quinoline Synthesis. *J. Organomet. Chem*. **2007**, 692, 4182–4186.

(29) Cho, C. S.; Seok, H. J.; Shim, S. C. A Rhodium-Catalyzed Route for Oxidative Coupling and Cyclization of 2-Aminobenzyl Alcohol with Ketones Leading to Quinolines. *J. Heterocycl. Chem.* **2005**, *42*, 1219–1222.

(30) Chelucci, G.; Porcheddu, A. Synthesis of Quinolines via a Metal-Catalyzed Dehydrogenative N-Heterocyclization. *Chem. Rec*. **2017**, 17, 200–216.

(31) Maji, M.; Chakrabarti, K.; Panja, D.; Kundu, S. Sustainable Synthesis of N-Heterocycles in Water Using Alcohols Following the Double Dehydrogenation Strategy. *J. Catal.* **2019**, *373*, 93–102.

(32) Xie, F.; Zhang, M.; Chen, M.; Lv, W.; Jiang, H. Convenient Synthesis of Quinolines from α-2-Nitroaryl Alcohols and Alcohols via a Ruthenium-Catalyzed Hydrogen Transfer Strategy. *ChemCatChem* **2015**, *7*, 349–353.

(33) Wang, Q.; Wang, M.; Li, H. J.; Zhu, S.; Liu, Y.; Wu, Y. C. Synthesis of Quinolines via Iron-Catalyzed Redox Condensation of Alcohols with 2-Nitrobenzyl Methyl Ether/2-Nitrobenzyl Alcohols. *Synthesis* **2016**, *48*, 3985–3995.

(34) Chun, S.; Putta, R. R.; Hong, J.; Choi, S. H.; Oh, D.C.; Hong, S. Iron-Catalyzed Transfer Hydrogenation: Divergent Synthesis of Quinolines and Quinolones from ortho-Nitrobenzyl Alcohols. *Adv. Synth. Catal.* **2023**, 365, 1 –9.

(35) Huang, S.; Hong, X.; Cui, H. Z.; Zhan, B.; Li, Z. M.; Hou, X. F. Bimetallic Bis-NHC-Ir(III) Complex Bearing 2-Arylbenzo[d]Oxazolyl Ligand: Synthesis, Catalysis, and Bimetallic Effects. *Organometallics* **2020**, *39*, 3514–3523.

(36) Quebatte, L.; Solari, E.; Scopelliti, R.; Severin, K. A Bimetallic Ruthenium Ethylene Complex as a Catalyst Precursor for the Kharasch Reaction. *Organometallics* **2005**, *24*, 1404–1406.

(37) Lam, R. H.; Keaveney, S. T.; Messerle, B. A.; Pernik, I. Bimetallic Rhodium Complexes: Precatalyst Activation-Triggered Bimetallic Enhancement for the Hydrosilylation Transformation. *ACS Catal* **2023**, *13*, 1999–2010.

(38) Laneman, S. A.; Stanley, G. G. Homogenous Transitions Metal Catalysed Reaction Advances in Chemistry, *American Chemical Society*, **1992**, 230, 350-366

(39) Diachenko, V.; Page, M. J.; Gatus, M. R. D.; Bhadbhade, M.; Messerle, B. A. Bimetallic N-Heterocyclic Carbene Rh(I) Complexes: Probing the Cooperative Effect for the Catalyzed Hydroelementation of Alkynes. *Organometallics* **2015**, *34*, 4543–4552.

(40) Fujita, H.; Takemoto, S.; Matsuzaka, H. Tin-Ruthenium Cooperative Catalyst for Disproportionation of Formic Acid to Methanol. *ACS Catal* **2021**, *11*, 7460–7466.

(41) Yuen, H. F.; Marks, T. J. Phenylene-Bridged Binuclear Organolanthanide Complexes as Catalysts for Intramolecular and Intermolecular Hydroamination. *Organometallics* **2009**, *28*, 2423–2440.

(42) Nishibayashi, Y.; Shinoda, A.; Miyake, Y.; Matsuzawa, H.; Sato, M. Ruthenium-Catalyzed Propargylic Reduction of Propargylic Alcohols with Silanes. *Angew. Chem., Int. Ed.*, **2006**, *45*, 4835–4839.

(43) Ammal, S. C.; Yoshikai, N.; Inada, Y.; Nishibayashi, Y.; Nakamura, E. Synergistic Dimetallic Effects in Propargylic Substitution Reaction Catalyzed by Thiolate-Bridged Diruthenium Complex. *J. Am. Chem. Soc.* **2005**, *127*, 9428–9438.

(44) Liu, T.; Chai, H.; Wang, L.; Yu, Z. Exceptionally Active Assembled Dinuclear Ruthenium(II)-NNN Complex Catalysts for Transfer Hydrogenation of Ketones. *Organometallics* **2017**, *36*, 2914–2921.

(45) Chai, H.; Liu, T.; Zheng, D.; Yu, Z. Cooperative N-H and CH2 Skeleton Effects on the Catalytic Activities of Bimetallic Ru(II)-NNN Complexes: Experimental and Theoretical Study. *Organometallics* **2017**, *36*, 4268–4277.

(46) Chai, H.; Wang, Q.; Liu, T.; Yu, Z. Diruthenium(II)-NNN Pincer Complex Catalysts for Transfer Hydrogenation of Ketones. *Dalton Trans.* **2016**, *45*, 17843–17849.

(47) Steiman, T. J.; Uyeda, C. Reversible Substrate Activation and Catalysis at an Intact Metal-Metal Bond Using a Redox-Active Supporting Ligand. *J. Am. Chem. Soc.* **2015**, *137*, 6104–6110

(48) Padmor, M. S.; Vishwakarma, P.; Tothadi, S.; Pratihar, S. Cooperative Bimetallic Co−Mn Catalyst: Exploiting Metallo-Organic and Hydrogen Bonded Interactions for Rechargeable C-/N-Alkylation. *ChemCatChem* **2023**, e202300828.

(49) Wehrmann, P.; Mecking, S. Highly Active Binuclear Neutral Nickel(II) Catalysts Affording High Molecular Weight Polyethylene. *Organometallics* **2008**, *27*, 1399–1408.

(50) Jangir, R.; Kaleeswaran, D.; Murugavel, R. 2,2′,6,6′-Tetraisopropylbenzidine-Based Sterically Encumbered Ditopic C2-Symmetric Ligand Systems and Supramolecular Building Blocks. *ChemistrySelect* **2018**, *3*, 8082–8094.

(51) R. Jangir, M. Ansari, D. Kaleeswaran, G. Rajaraman, M. Palaniandavar and R. Murugavel, Unprecedented Copper(II) Complex with a Topoquinone-like Moiety as a Structural and Functional Mimic for Copper Amine Oxidase: Role of Copper(II) in the Genesis and Amine Oxidase Activity. *ACS Catal.*, **2019**, *9*, 10940–10950.

(52) Gichumbi, J. M.; Friedrich, H. B.; Omondi, B. Synthesis and Characterization of Piano-Stool Ruthenium Complexes with N,N′-Pyridine Imine Bidentate Ligands and Their Application in Styrene Oxidation. *J. Organomet. Chem.* **2016**, *808*, 87–96.

(53) Bennelt, S. M.; Huang, T.; Matheson, T. W.; Smith, A. K. (η6-hexmethy lbenzene)ruthenium complexes;. *Inorganic Synth.*, **1982**, 21, 74-78.

(54) Deshmukh, G. D.; Rana, T. R. K.; Yadav, N.; Rajaraman, G.; Murugavel, R. Highly Active and Chemoselective Homobimetallic Ruthenium Catalyst for One-Pot Reductive Amination in Water. *Green Chem.* **2024**. https://doi.org/10.1039/D3GC03374K.

(55) Kayacı, N.; Dayan, S.; Özdemir, N.; Dayan, O.; Kalaycıoğlu Özpozan, N. One-Pot Stepwise Reductive Amination Reaction by N-Coordinate Sulfonamido-Functionalized Ru(II) Complexes in Water. *Appl. Organomet. Chem.* **2018**, *32* (12).

(56) Robles, O.; Romo, D. Chemo- and Site-Selective Derivatizations of Natural Products Enabling Biological Studies. *Nat. Prod. Rep*. **2014**, 31, 318–334.

(57) Hasdenteufel, F.; Luyasu, S.; Hougardy, N.; Fisher, M.; Boisbrun, M.; Mertes, P.-M.; Kanny, G. *Curr.Clin. Pharmacol.**2012***, 7, 15−27.

(58) Lobo, R. A. The Role of Progestins in Hormone Replacement Therapy. *Am. J. Obstet. Gynecol.* **1992**, *166*, 6, 1997–2004.

(59) Albuquerque, H. M. T.; Nunes da Silva, R.; Pereira, M.; Maia, A.; Guieu, S.; Soares, A. R.; Santos, C. M. M.; Vieira, S. I.; Silva, A. M. S. Steroid-Quinoline Hybrids for Disruption and Reversion of Protein Aggregation Processes. *ACS. Med. Chem. Lett.* **2022**, *13*, 443–448.

(60) Fitzpatrick, L. A.; Good, A. Micronized Progesterone: Clinical Indications and Comparison with Current Treatments. *Fertility and sterility*, **1999**, 72, 389-387.

(61) Albuquerque, H. M. T.; Nunes da Silva, R.; Pereira, M.; Maia, A.; Guieu, S.; Soares, A. R.; Santos, C. M. M.; Vieira, S. I.; Silva, A. M. S. Steroid-Quinoline Hybrids for Disruption and Reversion of Protein Aggregation Processes. *ACS. Med. Chem. Lett.* **2022**, *13*, 443–448.

(62) Sparapani, S.; Haider, S. M.; Doria, F.; Gunaratnam, M.; Neidle, S. Rational Design of Acridine-Based Ligands with Selectivity for Human Telomeric Quadruplexes. *J. Am. Chem. Soc.* **2010**, *132*, 12263–12272.

(63) Guo, Q. L.; Su, H. F.; Wang, N.; Liao, S. R.; Lu, Y. T.; Ou, T. M.; Tan, J. H.; Li, D.; Huang, Z. S. Synthesis and Evaluation of 7-Substituted-5,6-Dihydrobenzo[c]Acridine Derivatives as new c-KIT Promoter G-Quadruplex Binding Ligands. *Eur. J. Med. Chem.* **2017**, *130*, 458–471.

(64) Guo, B.; Yu, T. Q.; Li, H. X.; Zhang, S. Q.; Braunstein, P.; Young, D. J.; Li, H. Y.; Lang, J. P. Phosphine Ligand-Free Ruthenium Complexes as Efficient Catalysts for the Synthesis of Quinolines and Pyridines by Acceptorless Dehydrogenative Coupling Reactions. *ChemCatChem* **2019**, *11*, 2500–2510.

(65) *CrysAlisPRO*, Oxford Diffraction/Agilent Technol. UKLtd, Yarnton, Oxford, UK .L. J. Farrugia, *J. Appl. Crystallogr.*, 2012, **45**, 849–854.

(66) Dolomanov, O. V.; Bourhis, L. J.; Gildea, R. J.; Howard, J. A.; Puschmann, H. OLEX2: a complete structure solution, refinement and analysis program. *J. Appl. Crystallogr*. **2009**, 42, 339-341.

(67) Sheldrick, G. M. SHELXT: Integrating space group determination and structure solution. *Acta Crystallogr., Sect. A: Found. Adv* **2014**, 70, 1437

(68) Sheldrick, G. M. Crystal structure refinement with SHELXL. *Acta Crystallogr. C Struct. Chem*. **2015**, 71, 3-8.